Millimeter Wave Antenna Array Calibration and Validation for 5G New Radio Access

Manuel José López Morales
mjlopezmorales93@gmail.com

Department of EIT at Lund University
and
Ericsson AB in Lund

Supervisor: Professor Buon Kiong Lau

Ericsson AB Supervisors: Torsten Carlsson and Hans Hagberg

Examiner: Professor Mats Gustafsson

February 28, 2018

Printed in Sweden
Tryckeriet i E-huset, Lund

Theory is when you know everything but nothing works. Practice is when everything works but no one knows why. In our lab, theory and practice are combined: nothing works and no one knows why.

Crazy Proverb, Unknown Source

Abstract

This Master thesis work was performed in Ericsson AB, Lund. It studies and validates two classes of algorithms to be used in mm-wave massive MIMO antenna arrays, for their use in the future 5G mobile communication systems. The first class of algorithms relates to the calibration of the transceiver (TRX) chains responses of the antenna array and makes use of the antenna array mutual coupling, which is considered as known by the system. It is used to compensate for inaccuracies in the TRX base-band complex responses, caused by environmental conditions such as temperature, humidity and aging, which are much more critical in mm-wave than conventional bands. After the calibration, the beamforming capabilities of the massive MIMO systems are increased. The second class of algorithms is related to the estimation of antenna array mutual coupling matrix, due to the fact that this information is used in the first method. The antenna array mutual coupling estimation algorithm was proposed by Ericsson's engineers and tested in this work. Since the systems considered will work at mm-wave frequencies, small construction errors can create big differences in antenna array coupling properties, so the coupling matrix must be estimated for each constructed system of the same kind.

Several estimation and calibration algorithms were simulated, using Matlab® as a software for simulation, and analyzed. The estimation of TRX chains' complex responses is needed. Two estimation algorithms are used, referred as linear and non-linear least squares estimation. These estimation algorithms need to use the information regarding the antenna array mutual coupling matrix and over-the-air (OTA) self-measurements between pairs of elements in the antenna array. These measurements can be done considering all the possible pairs of elements in the antenna array (full measurements) or just a subset of the closest pairs (neighbour measurements). Firstly, simulations using a generic case were done, and later, simulations considering constraints in an Ericsson radio module proprietary system were done. Internal and external unwanted interference in the radio system were considered, to check for limitations in the estimation algorithms. So as to validate the proposed methods and algorithms, a testbed system using a radio module working at 28 GHz was built and measured. The signal levels and frequencies in the HW components of the testbed were calculated using the data-sheets of the components and later measured using a vector network analyzer and an spectrum analyzer. The last task was to write the code for con-

trolling the radio module, then perform calibration using it and finally measure the performance of the algorithm using an an-echoic chamber. Due to a lack of time, the code needed to do the OTA measurements, the OTA measurements and the validation of the algorithms are left as future work.

Observing the results of the simulations, several recommendations are made for future measurement validations. One common conclusion is that it is best to perform the minimum amount of self-measurements available, with those being the ones corresponding to the strongest coupling gains between elements in the antenna array. There were different preferred algorithms for calibration depending on the value of the signal-to-noise ratio (SNR) and the value of the signal-to-interference (SIR) ratio. Regarding the antenna array coupling matrix estimation, the conclusion is that the algorithm proposed by Ericsson's engineers works, but in order to achieve good results, the required post-processing SNR values of the related measurements may be too big. Therefore, it may take too long to perform these measurements. Possibilities to improve this algorithm are recommended and left as future work. Regarding the HW to be used in the testbed, it is recommended to add some extra components in order to improve the quality of the signals in the system, for future measurements.

Acknowledgements

People usually say personal advancement comes from a right mixture of intelligence and effort. I think this is true, but it does not only come from a combination of those two factors. For me, the most important factor is the people you surround yourself with, everyone you meet changes you and makes you who you are.

First of all, I would like to thank my academic supervisor, Professor Buon Kiong Lau for his support and help during the 5 months this project lasted. I am also grateful to my supervisors at Ericsson AB, Hans Hagberg and Torsten Carlsson, for their help and guidance during the project development. I felt very welcome since the very first day in the company. Special thanks to Krister Martini and Joakim Hallin, because their help in setting the testbed was nothing but priceless. Without all of them, it would not have been possible to finalize this project. My special thanks also go to Mr. Joao Vieira for his invaluable help and recommendations.

I thank all the people I have met since I started my university studies. All the guys from *Colegio Mayor Santo Tomás de Aquino*, specially to the closest ones, you made those tough first university years great. To the people in *Technical University of Madrid*: Rubén, Lian, José Manuel... with a special mention of Professor Manuel Sierra Castañer, your support and fruitful advice have been key to my personal and professional developments.

To the ones I think about everyday day: my father, who has always supported me and still does (he is still a superhero to me); my mother, who showed me the importance of effort and perseverance to achieve personal success; and my siblings. To my closest relatives: my uncle Paco, for convincing me to study a degree in Electrical Engineering, to my already deceased grandfather Francisco, who made me love Maths, and to my uncle José and my aunt Maru, it is great to share moments and conversations when I make a visit to Murcia.

To my Lund friends Santi "the personal trainer", Jaime, Álvaro, África, Tim, Alex, Cepeda, Cancela, Bea... you made my stay in Lund much more joyful and enriching. To my *murcian* and *alicantinian* friends Raúl, Alfredo, Jorge, Andrés, Luis, Quique and Ángel, it is amazing to share many laughters and good moments with you. And last but not least, to my love Marta, thanks for bringing happiness to my life.

Thanks to all the people I have met in my life, I am who I am because of you, and I do not regret any of it.

Popular Science Summary

Do you remember a time when you were watching a standard definition (SD) YouTube video or streaming a song on your laptop or PC and the player suddenly stopped? Nowadays you want to watch streaming videos on your laptop or mobile phone in a high-definition (1080p) format and in the future you may even want to stream 4K 3D videos and watch them in your Smart-TV or mobile phone. Mobile services are expected to be fast, reliable and cheap. Apart from this, the number of connected devices is growing exponentially, and three times more devices are expected to be connected in the next 5 years. Consequently, scientists and engineers are working towards developing and installing increasingly sophisticated systems to meet today's and tomorrow's user demands.

When it comes to cellular communications, there are several ideas on how to improve the network performance. Two of them are to have base stations with a lot of cooperating antennas and to use higher frequency bandwidths, only available at higher frequencies, in the millimeter wave region. These two concepts seem complicated, and they are! Nevertheless, these novel technologies are two main candidates to be integrated in future fifth-generation (5G) mobile systems, expected to be rolled-out in 2020.

When using multiple antennas in a base station (or even in a mobile device), it is desirable to avoid different behavior of the circuits in the system over time caused by temperature, humidity and other environmental factors. This is even more important when many antennas are used, as slight changes in the circuit responses may destroy the performance advantage of using these cooperating antennas. Everything gets even more complicated in higher frequencies, since the environmental effect is stronger. But Maths are really strong, and since all the data in our devices is in fact processed mathematically in a digital form, can't we do something to compensate for this physical (i.e. analog) effects in the mathematical (i.e. digital) domain?. The answer is yes, we can, and this mathematical compensation process is called calibration.

For the calibration procedure (or algorithm) to work, it is necessary to know how the many antennas interrelate to one another, for the different frequencies in the frequency band of interest. Hence, some antenna factory characterization must be done beforehand. Since this characterization gets more and more complex with an increasing number of antennas, and the antenna properties may still vary after installation, it is necessary to find more efficient methods of charac-

terization (in particular, efficient estimators of massive MIMO arrays coupling matrix). This Master thesis addresses these two problems associated with environmental changes effects in mm-wave massive MIMO systems and characterization of massive MIMO arrays.

List of Acronyms and Abbreviations

BS –> Base Station

CRLB –> Crammer-Rao Lower Bound

CSIN –> Cauchy-Schwartz Inequality

DL –> Down-link

DMR –> Deviation-to-mean Ratio

DSP –> Digital Signal Processor

DUT –> Device Under Test

IID –> Independent and Identically Distributed

FDD –> Frequency Division Duplexing

FPGA –> Field-Programmable Gate Array

FFT –> Fast Fourier Transform

GMM –> Generalized Method of Moments

IFFT –> Inverse Fast Fourier Transform

LLS –> Linear Least Squares

MIMO –> Multiple Input Multiple Output

mm-wave –> Millimetre Wave

NF –> Noise Fig.

NLLS –> Non-linear Least Squares

OTA –> Over-the-air

PAPR –> Peak to Average Power Ratio

RAM –> Random Access Memory

RF –> Radio Frequency

RFIC –> Radio Frequency Integrated Circuit

RX –> Receiver

SNR –> Signal-to-Noise Ratio

SIR –> Signal-to-Interference Ratio

TDD –> Time Division Duplexing

TRX –> Transceiver (Transmitter + Receiver)

TX –> Transmitter

UL –> Up-link

ZMCSCG –> Zero Mean Circularly Symmetric Complex Gaussian

Contents

List of Figures

List of Tables

Chapter 1

Introduction

During the past decade, the mobile communication market has grown tremendously and it is expected to continue doing so with more devices being connected every day. Apart from this, users demand higher data rates and new services, which need lower latency and more robust communications. Hence, 5G wireless communication standard [1],[2] is currently under development to meet these requirements. With a crowded frequency spectrum, the available bandwidth is limited and has to be shared between different users (e.g., cellular communications, broadcast services and radar). One way to serve more users is through the use of MIMO communications, originally proposed in [4] for increasing data rates. However, MIMO can also support multiuser communication in the same time and frequency resource. Multiuser MIMO has become an attractive option for practical implementation through the introduction of massive MIMO, advocating the use of very many antennas at the base station [5], [6]. MIMO technology consists of the use of multiple antennas on both transmitter and receiver to create multiple virtual data paths. Besides, since higher frequencies provide larger bandwidths, technologies working in these higher frequencies, called millimeter wave (mm-wave) frequencies [7], must be developed. Higher frequencies imply smaller antenna elements, which allow many more antennas to be placed in the same space, resulting in massive MIMO arrays. Thus, massive MIMO and mm-wave technologies go hand in hand [8]. Environmental factors, such as temperature and humidity, affect the performance of mm-wave massive MIMO systems. The focus of this Master thesis is to implement algorithms to reduce the effect of these environmental factors on mm-wave massive MIMO systems.

1.1 Background

Massive MIMO consists of the use of a greatly large number of antennas, in the range of hundreds and even thousands, that work together in order to increase the quality of the received signal, thus greatly increasing the wireless data transmission rates and energy efficiency. Mm-wave spectrum is the band of spectrum between 30 GHz and 300 GHz. This spectrum is considered as the way to provide 5G services due to the availability of more bandwidth to deliver faster, higher-quality video, and disruptive services.

Massive MIMO requires a very stable response of the transmit and receive radio frequency (RF) chains to work properly. Hardware impairments violate the requirement for flat transceiver (TRX) chains' responses and they may change with temperature, humidity or component aging [9]. Therefore, calibration algorithms for the compensation of non-idealities in the TRX chains' responses are needed. There are calibration algorithms for time-division duplex (TDD) operation [10] and frequency-division duplex (FDD) operation [11],[12],[13].

There is a problem that has not been fully addressed in mm-wave massive MIMO systems. The wireless channel between the transmitter and the receiver must be known by both sides of the communication link in order to achieve good beamforming capabilities. When the users first try to connect to a base station, they usually send a random access request in order to perform the procedures to get connected to the base station. In this very first stage, there is no previous knowledge of the channel. Hence, no beamforming can be made to the users in this stage. One solution to this problem is to beamform to a predefined set of directions, both in transmission and in reception. When the maximum signal is found in one of the preset directions, the user has been found by the base station, and, consequently, the base station is also found by the user. With this approach, users that are very far away from the base station can still get connected to it. Previously, the furthest users could not get connected because the received power was below the required threshold. The TX and RX chain responses must be estimated and compensated in the best possible manner, to avoid impairments which would destroy the beamforming capabilities. The TRX chains' calibration method proposed in this work can solve the aforementioned problem.

1.2 Objective

The goal of this Master thesis project is to study, implement and validate different calibration algorithms for compensation of hardware impairments in mm-wave massive MIMO systems. These calibration algorithms calibrate the downlink (DL) chain and the uplink (UL) chain of a base station, independently. To do so, the coupling matrix of the antenna array must be known. The higher the number of antenna elements, the harder it becomes to measure the array coupling matrix. The development of the thesis can be divided into three major milestones. Firstly, the study, simulation and selection of algorithms for array calibration. Secondly, the study, simulation and selection of algorithms for array coupling matrix estimation. Thirdly, the testing of these algorithms in an Ericsson AB proprietary testbed, located in Lund.

1.3 Methodology

Firstly, a literature study was performed in which the underlying theory and existing algorithms for TRX chains calibration were investigated [10],[11],[12],[13]. There are different algorithms that can be used for the calibration of the array TRX chains' responses. This thesis focuses on algorithms based on "self-measurements"

performed within the antenna array [17],[18],[19]. Different estimation algorithms were studied and simulated, and the most suitable one, for the problem at hand, was selected. MATLAB® was the tool used for these simulations.

Secondly, a literature study on array coupling estimation algorithms was also done [14]. Since the already existing algorithms are not as efficient as it is desirable, the chosen algorithm was the one developed internally in Ericsson, based on [20]. This algorithm is part of Ericsson intellectual property assets (IPA), so not all the implementation detail is disclosed. This algorithm is much faster and more efficient than the ones found in the literature. MATLAB® was the tool used for these simulations as well.

Lastly, a testbed for calibration and measurements on a real base station system was prepared, in order to check the validity of the algorithms proposed. The system is a radio module/ASIC developed by Ericsson [15],[16], and the measurements were done in an Ericsson testbed located in Lund. To control the testbed system, existing C# and Python control codes were modified.

1.4 Structure

The remainder of this report is structured as follows. In Chapter 2, an overview of calibration algorithms found in the literature is made. Different methods are explained, simulated and compared, and the most suitable method was selected. As well as this, the method proposed by Ericsson's engineers to estimate the coupling matrix of an antenna array is briefly explained. Chapter 3 shows simulations of different calibration techniques and simulations of the antenna array matrix coupling estimator algorithm. Chapter 4 describes the Ericsson base station system to be used, and the measurements to be performed in the testbed. Lastly, in Chapter 5, conclusions and suggestions for future work are provided.

Chapter 2
Algorithms and Estimators

2.1 TRX Chains Calibration Algorithms

MIMO systems can be used for three purposes: beamforming, spatial diversity and spatial multiplexing. The main purpose of a massive MIMO system is the last one. Spatial multiplexing in massive MIMO systems is performed by beamforming different signals to different users, located in different positions (this is also known as multiuser MIMO). Both line-of-sight and no-line-of-sight users are considered by massive MIMO. Beamforming can be done in azimuth and/or elevation by utilizing a proper antenna array (when it is made in both azimuth and elevation, it is known as 3D-beamforming). In Fig. 2.1, a conceptual comparison between beamforming in current mobile systems (single-user MIMO) and beamforming in 5G system (multiuser MIMO) is found.

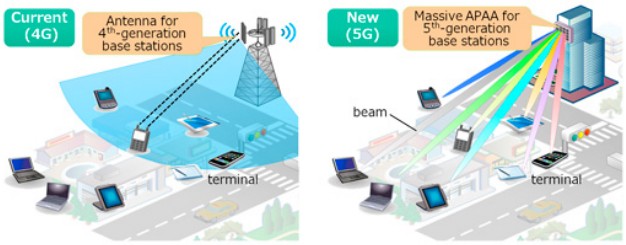

Figure 2.1: Example image. Reference [3]

Beamforming works by setting different amplitude and phase values on the electromagnetic (EM) surface currents of each antenna element, thus creating different interference in the far-field of different angular positions. This can be done by scaling signals in the base-band domain. It is generally agreed that the propagation channel is reciprocal [21], but the TRX RF chains at both ends of the link are generally not [22]. In mm-wave massive MIMO systems, amplitude and phase values must be set very accurately to beamform in the desired directions. Small errors in the phase values can lead to a complete loss of the transmission link. Therefore, a very accurate knowledge of the TX and RX chains' complex

responses is needed, in order to compensate for possible inaccuracies. Environmental conditions, such as temperature, humidity and components aging, result in changes of the TRX chains' responses. Hence, it is necessary to find a way to mitigate these effects. Isolated systems in terms of temperature, humidity and so on can be created. This kind of systems exist in more expensive and complex systems such as satellites or high performance radars, but are not affordable for mobile communications' base stations. That is the reason why the TRX chains' responses need to be calibrated. Such a procedure is termed "TRX calibration", and contains two steps: (i) estimation of calibration coefficients, and (ii) compensation by applying those coefficients to the TX/RX signals.

2.1.1 Description of Self-measurements

To estimate the TRX chains' responses at the base station side, a procedure named "self-measurements" must be performed. These measurements consist of sending a test signal through every transmit path to every receive path in the antenna system, using the mutual coupling between elements as propagation channel. This concept is illustrated in Fig. 2.2.

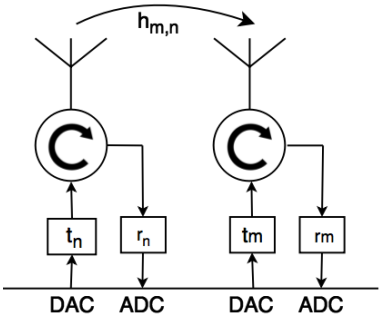

Figure 2.2: Self-measurements conceptual image.

Assuming the transmit (t_n and t_m) and receive (r_n and r_m) responses to include the response of the circulator in each direction, the signal model (i.e. digital equivalent signal) in this system for the path t_n to r_m through $h_{m,n}$ is

$$y_{m,n}(t) = r_m \cdot h_{m,n} \cdot t_n \cdot s_{test}(t) + n_{m,n}(t), \tag{2.1}$$

In Eq. 2.1, $y_{m,n}$ refers to the complex value obtained from the measurement between TX branch n and RX branch m, $n_{m,n}(t)$ refers to the noise in the measurement, not only captured by the antenna, but also generated by the receiver (thermal noise). The test signal s_{test} is defined over the time interval $0 \leq t \leq T_{sig}$, with T_{sig} being equal to the inverse of the minimum frequency component of the signal.

From the signal model, it can be observed that the higher the gain of the TX and RX responses, the higher the post-processing SNR. In section 3.1, it is seen that the higher this SNR, the better the calibration. Thus, self-measurements should be done by setting the amplifiers of the system to maximum gains but

also taking care that no component of the radio module is run into compression. Another way to increase the post-processing SNR is through performing the same measurement several times and then averaging over these measurements.

The array coupling matrix is assumed to be composed of a deterministic component $\overline{h}$ (coupling between antenna elements) and a random component $\widetilde{h}$, i.e. $h = \overline{h} + \widetilde{h}$. This random component is modeled as an independent and identically distributed (IID) zero-mean circularly-symmetric complex Gaussion (ZMCSCG) variable with variance $\sigma_{\widetilde{h}}$. The random component is used to model sources of interference such as reflections, internal circuits coupling, etc. It is supposed that only the deterministic component, which is the coupling between antenna elements, is known. The changes in the responses of the TX and RX chains are very slow (in the range of minutes). Since the length of the test signal is in the range of a few milliseconds, it is clear that the TX and RX chain responses can be taken as constant over the measurement time.

To estimate the calibration coefficients, one must sound the M antennas one-by-one by transmitting the test signal from each antenna and receiving on the other $M-1$ silent antennas. This makes a total of $M \cdot (M-1)$ measurements, which are expressed in matrix notation in Eq. 2.2,

$$\mathbf{Y}(t) = \mathbf{R} \cdot \mathbf{H} \cdot \mathbf{T} \cdot s(t) + \mathbf{N}(t), \tag{2.2}$$

where $\mathbf{H} = \mathbf{H}^T$ is assumed. Estimation algorithms need the same or a higher number of equations, compared to the number of (unknown) variables, to work. Since there are a total of $2M$ variables to estimate, at least $2M$ equations are needed. Therefore, some measurement combinations may be unnecessary. Since the goal of estimation algorithms is to find out which parameters are more likely to be present in a set of functions, which must be defined before using them in estimation algorithms. There are different possibilities, but we focused our study on three cases: full measurements, neighbour measurements and weighted measurements.

Full Measurements

There are a total of $M \cdot (M-1)$ available measurements that can be used. In Fig. 2.3, one can find a conceptual image of all the measurements available from a central element, in a 5 by 5 array. There are advantages and disadvantages when using this full set of measurements. It may seem that the higher the number of available measurements, the better the estimation. This is true in case the measurements have a good enough post-processing signal-to-noise ratio (SNR) and signal-to-interference ratio (SIR). This is not true for the furthest elements in the antenna array. To overcome this issue, another interesting approach is described in the next section, which consists of using a (neighbour) subset of all the possible measurements.

Neighbour Measurements

There must be more than $2M$ raw measurements, but not necessarily $M \cdot (M-1)$, hence, the estimation can be performed using a lower number of measurements

with respect to all the combinations. This number must be N_{meas}, with $2M \leq N_{meas} \leq M(M-1)$. Since $2M \leq M(M-1)$, M must be higher than or equal to 3. Measurements can be performed from all the elements to a subset of elements, such as their neighbours. In Fig. 2.4, one can find an illustration of a reduced set of measurements, called neighbour measurements, with the 4 closest neighbours (of the central element) in the planar array being considered.

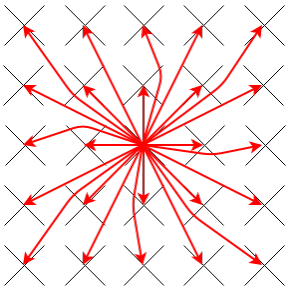

Figure 2.3: All measurements.

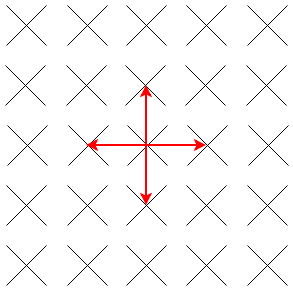

Figure 2.4: 4 neighbour measurements.

One advantage of neighbour methods is that they are much faster, since fewer measurements are needed and the estimation algorithms only need to compute a lower amount of data.

Weighted Measurements

Another possibility is to define a set of weighted functions, weighting them proportionally to the expected SNR per measurement. Weighted equations must always be defined so that they agree with the signal model definition. This is not as straightforward as selecting a subset of functions. Weighted measurements' functions for relative DL-to-UL calibration were defined in [10]. Weighted measurements for absolute DL (TX) and absolute UL (RX) estimation is so complex it is out of the scope of this thesis. One possibility is to combine weighted measurements with neighbour measurements, hence improving the results by eliminating measurements with extremely low SNR and reducing the impact of measurements with low SNR while increasing the impact of the most reliable (high SNRs) measurements.

2.1.2 Estimation Methods

Generalized Method of Moments

This method was originally introduced for statistical inference in econometrics. It is an estimation approach which exploits a particular structure of the signal model, more specifically the *moment conditions* [23]. In our case, a vector of moment conditions $\mathbf{g}(y, r, t)$ that satisfies $E\{\mathbf{g}(y, r, t)\} = E\{\mathbf{g}(y, \phi)\} = \mathbf{0}$ is required, where $\mathbf{0}$ is an all-zeros vector. In the previous equation, $\mathbf{r} = [r_1 \dots r_M]^T$, $\mathbf{t} =$

$[t_1 \dots t_M]^T$, $\phi = [\mathbf{t}^T \mathbf{r}^T]^T$ and $\mathbf{y} = [{y_{1,2}}^T \dots {y_{1,M}}^T \quad {y_{M,1}}^T \dots {y_{M,M-1}}^T]^T$. Defining the moment conditions to be Eqs. 2.3 and 2.4,

$$E\{f_{n,m,l}\} = E\{y_{m,l} r_n h_{n,l} - y_{n,l} r_m h_{m,l}\} \quad \forall m,l,n \quad \text{and} \quad m \neq n \neq l, \tag{2.3}$$

$$E\{d_{n,m,l}\} = E\{y_{l,m} t_n h_{l,n} - y_{l,n} t_m h_{l,m}\} \quad \forall m,l,n \quad \text{and} \quad m \neq n \neq l, \tag{2.4}$$

and stacking all $f_{n,m,l}$ terms in $\boldsymbol{f}(y,r)$ and all $d_{n,m,l}$ terms in $\boldsymbol{d}(y,t)$, and denoting

$$\boldsymbol{g}(y,\phi) = [\boldsymbol{f}(y,r)^T \ \boldsymbol{d}(y,t)^T]^T, \tag{2.5}$$

the GMM estimator is obtained by solving

$$\phi_{est} = arg \min_{\substack{\phi \\ \|\mathbf{t}\|^2 = M \\ \|\mathbf{r}\|^2 = M}} \mathbf{g}(y,\phi)^H \cdot \mathbf{W} \cdot \mathbf{g}(y,\phi), \tag{2.6}$$

where $\mathbf{W}$ is a weighting matrix that generally needs to be optimized. Note that the imposed constraints avoid the all-zero solution and normalizes the average energy per entry of ϕ_{est} to one. The GMM method can be solved by using optimization algorithms.

Linear Least Square (LLS) Methods

The linear least square methods are a particularization of the GMM. By setting $\mathbf{W}$ to be the identity matrix, Eq. 2.6 results in $\phi_{est} = arg \min_\phi \|\mathbf{g}(y,\phi)\|^2$, which can be solved by fitting this equation to a M-dimensional line, through the linear least square approximation. To include the power constraints $\|\mathbf{t}\|^2 = M$ and $\|\mathbf{r}\|^2 = M$, this method must be solved by using Lagrange multipliers [24]. The Lagrange function is defined as

$$L(x,\lambda) = \|\mathbf{g}(y,\phi)\|^2 + \lambda_1(\|t\|^2 - M) + \lambda_2(\|r\|^2 - M), \tag{2.7}$$

and to solve the problem, the gradient $\nabla_{x,\lambda}(x,\lambda)$, must be computed and set to zero. Then, solutions to this equality must be found. Since this method seemed a bit complicated (and time consuming) from Ericsson's perspective, the recommendation was to use a method already developed in the company. It consists of using the formula $y_{n,m} = r_n \cdot (\bar{h}_{n,m} + \tilde{h}_{n,m}) \cdot t_m + n_{n,m}$. For the high signal quality case ($SNR \to \infty$ and $SIR \to \infty$), the equation simplifies to $y_{n,m} = r_n \cdot \bar{h}_{n,m} \cdot t_m$. One can then define

$$\Gamma_{n,m} = \frac{\bar{h}_{n,m}}{y_{n,m}} = \frac{1}{r_n} \cdot \frac{1}{t_m} \to \Gamma_{n,m} \cdot t_m - \frac{1}{r_n} = 0. \tag{2.8}$$

Eq. 2.8 can be re-written in matrix form as $\mathbf{A} \cdot \mathbf{x} = \mathbf{b}$. A is composed of elements of $\Gamma_{n,m}$ and some "-1"s, $\mathbf{x}$ contains the unknowns t_m and $\frac{1}{r_n}$, and $\mathbf{b}$ is

forced to have one element different from zero, to avoid the all-zero solution. Vector **x** is calculated as

$$\mathbf{x} = (\mathbf{A}^T \cdot \mathbf{A})^{-1}\mathbf{A}^T \cdot \mathbf{b} \tag{2.9}$$

This method requires a matrix inversion. The detailed derivations of this matrix and vectors are given in Appendix A.1. This method estimates the RX and TX chain responses, scaled by an unknown complex constant which appears since one of the parameters is forced to take the value of 1. There were two possibilities for defining Eq. 2.8, by defining $\Gamma_{n,m} = \frac{\overline{h}_{n,m}}{y_{n,m}}$ or by defining $\Gamma_{n,m} = \frac{y_{n,m}}{\overline{h}_{n,m}}$. In Appendix A.1, it is demonstrated that the first definition leads to a higher post-processing SNR of the estimation. In case it is one's intention to calculate the relative RX/TX chain responses, Eq. 2.8 must be defined as Eq. 2.10.

$$\Gamma_{n,m} = \frac{\overline{y}_{n,m}}{y_{m,n}} = \frac{r_m}{r_n} \cdot \frac{t_n}{t_m} = \frac{c_m}{c_n} \rightarrow \Gamma_{n,m} \cdot c_n - c_m = 0. \tag{2.10}$$

Non-linear Least Square (NLLS) Method[1]

This approach consists of using the Gauss-Newton minimization algorithm. One must define a set of equations in vector form as $f(x) = \mathbf{0}$, as it is shown in Eq. 2.11.

$$\begin{bmatrix} f_1(x) \\ f_2(x) \\ \vdots \\ f_K(x) \end{bmatrix} = \begin{bmatrix} 0 \\ 0 \\ \vdots \\ 0 \end{bmatrix} \tag{2.11}$$

where **x** is the vector of unknowns. The vector **x** can be found by iterations as

$$\mathbf{x}_{l+1} = \mathbf{x}_l - \mathbf{J}(x_l)^+ \mathbf{f}(x_l), \tag{2.12}$$

where $\mathbf{J}^+$ is the pseudo-inverse of the Jacobian matrix. As well as this, one element of the Jacobian matrix is defined as $[\mathbf{J}(x_l)]_{mn} = \frac{\partial f_m}{\partial x_n}$, where $m = 1, \ldots, M$ (M is the number of equations), $n = 1, \ldots, N$ (N is the number of unknowns) and the Jacobian matrix equals $\mathbf{J}(x_l)^+ = (\mathbf{J}(x_l)^T\mathbf{J}(x_l))^{-1}\mathbf{J}(x_l)^T$.

By using the definition of the signal model found in Eq. 2.8, and by defining $f_{n,m} = \Delta_{n,m} - \delta t_m \cdot \delta r_n$, with $\Delta_{n,m} = \frac{\overline{h}_{n,m}}{y_{n,m}}$, $\delta t_m = \frac{1}{t_m}$ and $\delta r_n = \frac{1}{r_n}$, one has all the equations needed to solve the problem. The detailed derivation of these matrices and vectors are provided in Appendix A.2. Since the solution for this method requires the pseudo-inversion of a matrix, it consumes a high computational load.

One suggestion is to solve this equation by using quasi-Newton methods [20], because these methods are computationally more efficient. As seen in Appendix B.1, this method estimates the RX/TX chain responses scaled by an unknown complex constant. This same problem occurred in the LLS estimation approach.

[1]The application of non-linear least squares approximation as an estimation method was proposed by Ericsson's engineers at the end of 2016.

2.1.3 Further Issues on Calibration

Two-Stage Calibration

Two calibration stages are found in any base station system:

1. Initial installation's calibration setup.
2. On-the-go calibration: this is done when the system is working, sending and receiving data to and from users.

In the first case, the deviation of the TRX chains' responses (to be called "error" from now on) is uncontrolled, and may be extremely big. Despite that, several minutes can be allocated for the base station system to set itself up in a real installation scenario, so one can overcome the big initial error.

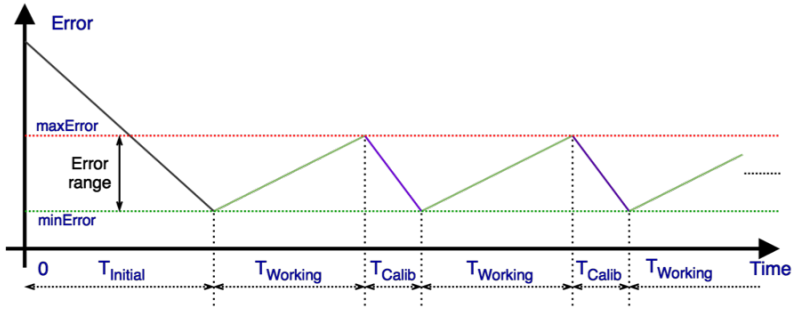

Figure 2.5: Timing scheme for the two stage calibration procedure.

In the second case, the error is controlled and limited to a maximum acceptable value. Since the minimum achievable error depends on the SINR, as will be seen in section 3.1, a minimum value for this error must also be chosen. The error is expected to increase in a linear fashion (this is just an assumption for simplicity). Thus, considering maximum and minimum errors, time periods can be estimated. A timing scheme is illustrated in Fig. 2.5. In this image, the meaning of the variables are:

- $T_{Initial}$: calibration time for system initialization.
- $T_{Working}$: time during which the system sends/receives users' data and does not need to perform calibration.
- T_{Calib}: time the system needs for calibration of the circuits in the TRX chains. Users are idle during this time.

In Fig. 2.6, a conceptual image of the cluster of uncalibrated (red) and calibrated (green) complex values in the initialization calibration is found. In Fig. 2.7, a conceptual image of the cluster for the on-the-go calibration is found. One must be aware of the different scalings of the x and y axes. The distributions of these clusters are directly related to the DMR (deviation to mean ratio) performance tool, to be elaborated in Section 2.3.3.

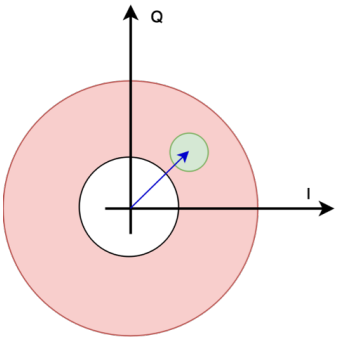

Figure 2.6: Cluster of TRX chain baseband complex responses for setup calibration.

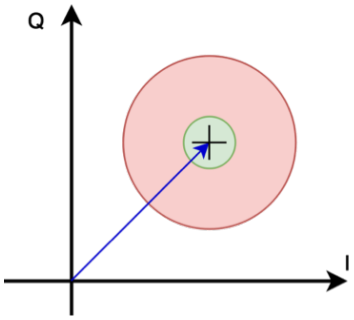

Figure 2.7: Cluster of TRX chain responses for on-the-go calibration.

Let's clarify DMR with an example. Consider a maximum deviation of one degree per radius of value 1, i.e.

$$DMR = \frac{1deg \cdot (\pi/180)}{1volt} \rightarrow DMR(dB) = 20 \cdot log_{10}(\frac{\pi}{180}) = -35\ dBc. \quad (2.13)$$

If the minimum desired DMR is set to be a tenth of the maximum acceptable error, the minimum DMR will be -45 dBc. All these DMRs can be obtained under certain post-processing SIR and SNR constraints. In the next chapter, simulations are done in order to choose the post-processing SIR and SNR values that result in the desired DMR values.

Iterative Calibration Procedure

The possibility of performing more than one calibration calculation per calibration procedure was considered and tested. Instead of only doing one measurement and then calibrate, the idea is to perform one measurement and one calibration, more than once. This concept is further developed in Section 5.2.1. This option was considered in case the calibration procedure is not only limited by post-processing SNR and/or SIR but also by the capabilities of the calibration method. In Chapter 3, one can find simulations that consider two calibration calculations per calibration procedure.

Importance of Phase Compensation

The non-idealities in the circuits of the TRX chains affect the equivalent currents on the antennas' surfaces of the massive MIMO array. By changing the amplitude of the equivalent currents on the antenna surface, over the array aperture, the main lobe angular width and side-lobe-levels (SLLs) can be modified [21]. By

changing the effective phase of the currents over the array aperture, a change in the main-beam pointing direction of the array pattern is achieved.

Hence, the compensation of the phase component is much more important than compensation of the amplitude component, for mm-wave massive MIMO application. If the calibration method is able to get an "almost flat" response of the phase values of the complex TRX circuits' responses, but a not "so flat" response of the amplitude values, the calibration can be still regarded as valid. In Chapter 3, it can be seen that calibration algorithms better compensate the phase component of the TRX circuits' responses than the amplitude component.

2.1.4 Types of Compensation

Once the TRX circuits' base-band complex responses have been estimated, they must be compensated in order to achieve the desired beamforming properties. There are three different types of compensation, depending on the kind of system used: switched array (relies on analog compensation), fully digital array (relies on digital compensation) and hybrid array (relies on analog or hybrid compensation).

Fully Digital Array (Digital Compensation)

If a fully digital array (one RF chain per antenna element) is used, the calibration can be done in the digital domain. This compensation consists of "pre-multiplication" by the inverse value of the estimated complex response of each TRX chain, in each base-band port. For example, to beamform power in a certain direction, the signal to send through each antenna port "n" will be s_n^{beam}. If the estimated complex transmit response in each TX chain is t_n, the effective signal to send through each port must be $s_n^{eff} = \frac{1}{t_n} \cdot s_n^{beam}$. As shown in Fig. 2.8, the compensation in a fully digital array can be completely done in the base-band digital domain. For a fully digital array, each DAC and ADC port are fully free to set any scaling coefficient to the signals sent from and to them.

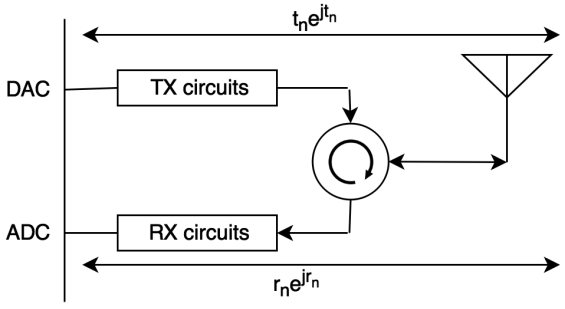

Figure 2.8: Schematic idea of a TRX circuits' digital compensation.

Switched Array (Analog Compensation)

When using switched arrays, which perform analog beamforming through the use of power amplification and phase shifting in each antenna element, the compensation must be done in the analog domain. The compensation in these systems is much more complicated than in a fully digital array:

- Power amplification compensates for the amplitude component of the TRX chains' complex responses.
- Phase shifter compensates for the phase component of the TRX chains' complex responses.

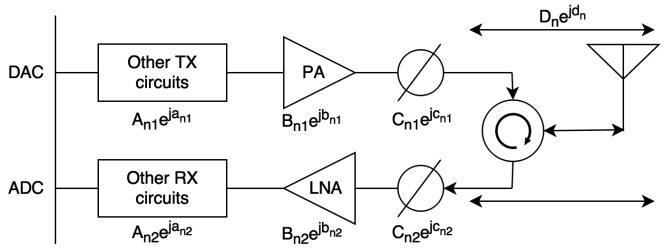

Figure 2.9: Schematic idea of a TRX circuits' analog compensation.

Different configurations of the power amplifier generate different phase responses. Different configurations of the phase shifter generate different gain/loss responses. Hence, the operations of amplification and phase shifting cannot be considered as linear. There are two ways to solve this problem:

- Predefined tables: stored configurations where the full response (amplifiers + phase shifters) is known beforehand. This can result in a huge memory consumption.
- Control loop: this requires the use of a measurement probe in each antenna port. Then, a control loop is applied, to re-adjust the signal until the desired values are obtained. This solution scheme is shown in Fig. 2.10.

From Fig. 2.9, it can also be understood that the compensation is not linear. The overall response of the chain is affected by the amplifiers, the phase shifters, the connection to the antenna as well as tho connection of the circuits to the digital base-band domain. The calibration must be done by taking into account the configuration in which the amplifier and phase shifter were set during the self-measurement procedure. In the radio module used in this work, the compensation is done in the analog domain, so further work is needed in order to define the corresponding calibration algorithm.

2.2 Antenna Coupling Matrix Estimators

For the calibration algorithms to work, it is necessary to use the antenna array coupling matrix. With a few antennas, this coupling matrix can be estimated

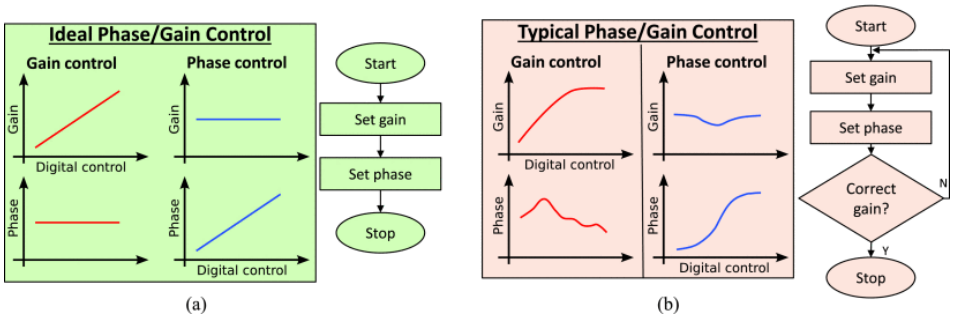

Figure 2.10: (a) Ideal case, (b) Gain-phase balancing by using a control loop. This image can be found in [15].

using scattering parameters and a vector network analyzer [25]. This is affordable if there are just a few antennas in the system. With many antennas, this procedure gets really complicated. Another approach to estimate the coupling matrix is by performing measurements in an anechoic chamber in different angular positions [14]. Since all the existing methods take too much time and may not be affordable for certain cases, such as the one in this work, an innovative estimation method, which is proposed by Ericsson's engineers, will be simulated and verified.

2.2.1 Procedure for Matrix Estimation[2]

The estimation of the coupling matrix must be done during factory calibration. The steps for the proposed method are:

1. Estimate receiver paths in the device-under-test (DUT) radio unit.
2. Measure internal coupling between digital ports (self-measurements).
3. Estimate antenna coupling matrix based on step one and 2.

RX Paths Estimator in DUT

The DUT and probe, i.e. test transmitter, must be placed in an anechoic chamber, with a distance enough to assume far-field distance, i.e. the incident plane wave, between DUT and probe. The probe is physically positioned to ensure that the incident plane wave gives identical incident signals at each antenna element on the DUT antenna array (i.e., probe being placed in the broadside direction of the array). The antennas must then be perfectly positioned and aligned, with respect to each other. A conceptual image can be found in Fig. 2.11.

Then, a test signal TX_{test} is sent over-the-air from the probe to the DUT. The received signal at each antenna port is equal to $k_1 \cdot TX_{test}$, where k_1 is the unknown path between the DAC port in the test transmitter and antenna ports in the antenna array. In Fig. 2.12, a full detailed scheme for the plane wave acquisition is illustrated.

[2]This procedure is proposed by Ericsson's engineers.

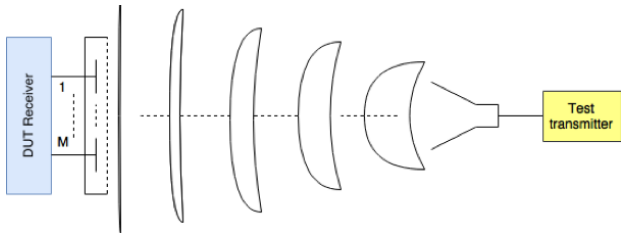

Figure 2.11: Plane wave acquisition by DUT.

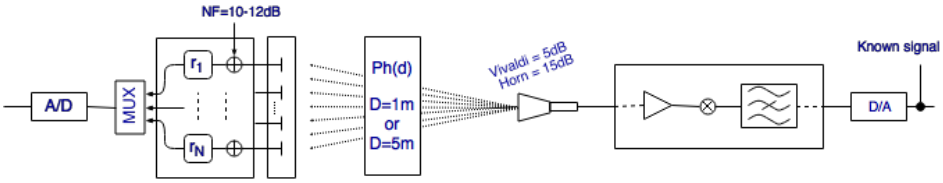

Figure 2.12: Full propagation path for plane wave acquisition by DUT.

Note that there may be a small impact on the received signals from antenna coupling. If needed, the simulated antenna coupling array can be used to correct the received signals. The assumption is that it is not needed since all the antennas receive identical signals and hence coupling between them should not influence the measurements. Receiver algorithms may be used to mitigate impact from unwanted reflections in the test room, since they can isolate line-of-sight wave from the reflected incident waves. The total transfer functions between the transmitter and receiver is given in Eq. 2.14 and a conceptual image of the equivalent base-band complex RX chains' responses of the DUT is provided in Fig. 2.13.

$$y_i = \frac{RX_i}{TX_{test}} = k_1 \cdot r_i. \tag{2.14}$$

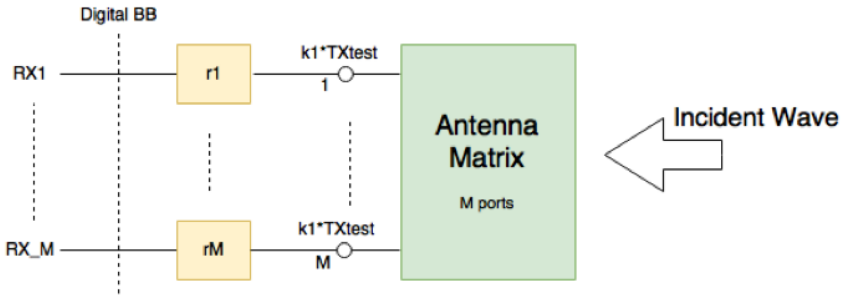

Figure 2.13: Signal view from plane wave acquisition.

It is convenient to remove any unknown attenuation/gain in the estimated receiver functions by scaling the estimates. One proposal is to scale to have the

RMS signal of the receiver functions to equal to 1. Each receive function $\hat{r}_i$, as defined in Eq. 2.15, will then show the deviation from the ideal signal,

$$\hat{r}_i = y_i \cdot \frac{M}{\sum_{k=1}^{M} |y_k|^2}. \tag{2.15}$$

It may be possible to rotate the DUT to get other incident angles. These measurements can give information on the physical placement of the antenna patches in the antenna matrix. This information can be used to compensate for errors in the physical placement when the antenna matrix is used for fixed beam communication. There is a small difference in the received power, and a big difference in the received phase, in each antenna element in the DUT array. Considering the DUT as a circular aperture of radius R, measuring at a distance D_{meas}, the effective distance between the probe and the DUT aperture edge is $D_{edge} = \sqrt{D_{meas}^2 + R^2}$. Between the aperture edge and aperture center, there is a difference in the received power of

$$PW_{diff} = 10 \cdot log_{10}(D_{edge}) - 10 \cdot log_{10}(D_{meas}), \tag{2.16}$$

and a phase difference of

$$\phi_{diff} = \frac{2\pi}{\lambda} \cdot (D_{edge} - D_{meas}). \tag{2.17}$$

For the smallest far-field distances, the angular aperture from the DUT center to the DUT edge ($\theta = \arctan(R/D_{meas})$) is around 3-4 degrees. Therefore, no radiation pattern compensation is needed. For the smallest far-field distances, the difference in the received power between the antenna center and the antenna edge is in the order of tenths of a dB (even lower), so it can be neglected. However, the phase difference caused by the different propagation distances must be calculated and compensated in the mm-wave frequency range. An aperture with a radius of 4cm, at a measurement distance of one meter, and a working frequency of 28 GHz, gives a phase difference of 0.47 radians, i.e. 27 degrees. Hence, the crucial effect to compensate is the phase difference caused by different propagation distances. This correction is named "parallax error correction" in Ericsson.

Self-Measurements

The DUT has to be placed in a physical environment where signals from unwanted reflections in the room are significantly smaller than the signal in the direct path. Anechoic chamber is not needed but since it is used in the previous step, the proposal is to continue with the same environment. The time between the measurements in the previous and the current steps should be small enough to ensure that the DUT is behaving in the same way in both steps. The signals are injected into one digital base-band port and received at a different digital base-band port. These self-measurements must consider all the possible combinations of measurements in order to estimate as many antenna array coupling values as possible. It is possible to receive at multiple ports using the same transmit port. It may be even possible to transmit from multiple ports simultaneously if one can

create orthogonal signals in each transmitter by using orthogonal codes. The total transfer function from port j to port i is:

$$y_{ij} = \frac{RX_i}{TX_j} = r_i \cdot h_{ij} \cdot t_j + n_{ij}. \tag{2.18}$$

Estimator of Antenna Coupling

Two options are considered for antenna coupling estimation. The first option consists of using an already published method for relative RX/TX chain response estimation. The selected method is the LLS. It contains the following steps:

1. Estimate the relationship between the RX/TX transfer functions $\hat{c_i} = r_i/t_i$. The methods are published in [12]. In this work, we have to solve a matrix problem based on the following formulation:

$$\Gamma_{nm} = \frac{Y_{nm}}{Y_{mn}} = \frac{r_n \cdot t_m}{r_m \cdot t_n} = \frac{c_n}{c_m} \rightarrow \Gamma_{nm} \cdot c_m - c_n = 0. \tag{2.19}$$

2. Calculate the transmit transfer function as $\hat{t_i} = \hat{r_i}/\hat{c_i}$, with scaling such that $\frac{1}{M}\sum_{k=1}^{M} |\hat{t_k}|^2 = 1$
3. Estimate antenna coupling matrix. Note that there are $M(M-1)/2$ coupling coefficients in an antenna matrix with M ports.
   (a) Each antenna coupling h_{ij} can be extracted from two self-measurements $y_{ij} = r_i \cdot h_{ij} \cdot t_j$ and $y_{ji} = r_j \cdot h_{ji} \cdot t_i = r_j \cdot h_{ij} \cdot t_i$.
   (b) Using the estimated values $\hat{r_i}$ and $\hat{t_i}$, we get $\hat{h_{ij}} = \frac{y_{ij}}{\hat{r_i} \cdot \hat{t_j}}$ and $\hat{h_{ij}} = \frac{y_{ji}}{\hat{r_j} \cdot \hat{t_i}}$, which are combined to increase the post-processing SNR of the estimation by a maximum of 3dB.

The second option consists of the estimation of the antenna coupling matrix directly from plane wave acquisition and self-measurements. This option is most likely the better option since intermediate results tend to increase uncertainties. Regarding this option, several alternatives exist. By considering three ports k, l, m, with one signal transmitted from port l and received at ports k and m, the signal models are written in Eq. 2.20:

$$y_{kl} = r_k \cdot h_{kl} \cdot t_l + n_{kl} \quad and \quad y_{ml} = r_m \cdot h_{ml} \cdot t_l + n_{ml}. \tag{2.20}$$

One can eliminate the unknown transmitter parameter t_l and rewrite the formula as given in Eq. 2.21:

$$res_{klm} = y_{kl} \cdot r_m \cdot h_{ml} - y_{ml} \cdot r_k \cdot h_{kl}, \tag{2.21}$$

with expected value $E(\widehat{res_{klm}}) = 0$. There are multiple ways to solve these equations, such as NLLS newton-method, LLS method, maximum-likelihood (ML) method, etc. In this Master thesis work, two methods were tested for option 2, LLS estimation and NLLS estimation.

2.2.2 Further Issues in Coupling Matrix Estimation

Effect of the Unknown Constant

During the estimation of the RX circuits' complex response vector, when normalization is done, the estimated RX complex response would be $\hat{r} = k_1 \cdot r$. When the relative DL to UL complex response is estimated, another unknown constant appears. Since the TX circuits' complex response equal

$$\hat{t} = \frac{\hat{r}}{\hat{c}} = \frac{k_1}{k_2} \cdot \frac{r}{c} = k_3 \cdot t, \tag{2.22}$$

when the antenna array coupling matrix is estimated, a total scaling factor affects the estimation. This effect is shown in Eq. 2.23

$$\hat{h}_{ij} = \frac{y_{ij}}{\hat{r}_j \cdot \hat{t}_i} = \frac{y_{ij}}{k_1 \cdot k_3 \cdot r_j \cdot t_i} = k_T \cdot h_{ij}. \tag{2.23}$$

This is not a problem if the scalar k_T is the same for all the estimated values. The ratios between different antenna coupling values h_{ij}/h_{kl} must be kept the same as if there is no uncontrolled scaling. The scaling is removed by applying normalization to the estimated antenna array coupling matrix values. After estimating the coupling matrix, it is our goal to use it for TX and RX circuits' calibration. The estimated antenna array coupling matrix has the following structure $\hat{h}_{ij} = k_T \cdot (h_{ij} + \mu_{ij})$, where μ_{ij} is the noise present in the estimation when h_{ij} is estimated by using two consecutive and independent noisy measurements. Since the estimation of the coupling matrix is not time-critical, the post-processing SNR of both measurements could be greatly increased. For low SNR in the plane wave acquisition's measurements and without the normalization of the estimated antenna array coupling matrix, by observing the full signal model $(y_{ij} = r_i \cdot (k_T \cdot (h_{ij} + \mu_{ij})) \cdot t_j + n_{ij})$, it can be understood that the quality of the self-measurements will be drastically reduced.

Estimator of H_{eff}

As it was explained in Section 2.1.1, there is a random component in the antenna array coupling matrix of the signal model for the self-measurements, i.e. the interference related term $\widetilde{h}$. The calibration procedure will be severely affected in the case of low post-processing SIR. Hence, there is a strong limitation coming from multiple unknown sources of interference, but this problem can still be reduced. If the interference is considered as reciprocal, i.e., $I_{nm} = I_{mn}$, and to be invariant over time and environmental conditions, an "effective" coupling matrix $H_{eff} = H + I$ can be estimated.

The interference matrix may be composed of the sum of a deterministic component and a varying component, i.e. $I = I_{det} + I_{var}$. Averaging over several calculations of this effective matrix may reduce the size of the varying component. When using the "effective" estimated coupling matrix for the calibration procedure, the effect of the interference will be much lower. It is very important to remark that in order to estimate the effective coupling matrix H_{eff}, two conditions must hold:

- The interference matrix must be reciprocal ($I = I^T$).
- The interference matrix must be time invariant and not affected by environmental conditions.

When a base station system is placed "on-site", there will still be a small source of interference due to reflections from the surroundings. One must consider that interference will always be present in any real system.

2.3 Performance Measures

In order to select the best estimation method to be applied for the calibration of the TRX circuits, performance measures must be defined. Below, several performance measures are defined for the estimation of the TRX circuits' responses.

2.3.1 Cramér-Rao Lower Bound

The CRLB indicates the theoretical lower boundary of the variance of any unbiased estimation of an unknown parameter based on observed data, which depends directly on this unknown data. Thus, it defines a lower bound on the variance of any unbiased estimator of $\phi_{est} = [\hat{\mathbf{t}}_{est}^T \hat{\mathbf{r}}_{est}^T]^T$. It can be used as a reference of the best possible estimation of the given parameters. Its derivation for the case at hand is extremely complicated, and it is out of the scope of the Master thesis. A full mathematical derivation can be found in [11]. Since it is not critical to obtain an absolute comparison against the "best" possible performance, given by the CRLB, just a relative comparison between several methods is sufficient.

2.3.2 Mean Square Error

The mean square error (MSE) between the uncalibrated TX/RX chain responses and their estimations is another performance measure. Since the estimated parameters are scaled by the same unknown constant, one must define the MSE in a way that this constant is removed. The simplest way to solve this is by dividing all the estimated parameters by one of them, hence removing the unknown constant. A division by the corresponding parameter must be done on the initial values, in order to scale both sets of parameters accordingly. The estimation method with the lowest MSE is the best in terms of the estimation performance. The MSE for the RX and TX chain responses are given in Eq. 2.24.

$$MSE_{\hat{\mathbf{r}}} = E_{\mathbf{r}}[(\mathbf{r} - \hat{\mathbf{r}})^2] \quad and \quad MSE_{\hat{\mathbf{t}}} = E_{\mathbf{t}}[(\mathbf{t} - \hat{\mathbf{t}})^2]. \tag{2.24}$$

2.3.3 Cauchy Schwartz Inequality

Since the estimated parameters are scaled by an unknown constant, a performance measure that does not need to explicitly deal with this scaling factor is of interest. The Cauchy-Schwartz inequality (CSIN), which states how "parallel" two n-dimensional vectors are, can do this. The formulation of the CSIN for the

RX and TX chain responses is illustrated in Eq. 2.25, where $\hat{r}$ and r are the estimated RX and original RX circuits' responses, and $\hat{t}$ and t are the estimated TX and original TX circuits' responses, respectively. This is shown in Eq. 2.25.

$$0 \leq r_{cs} = \frac{\sqrt{|r^H \cdot \hat{r}|}}{\|r\| \cdot \|\hat{r}\|} \leq 1 \quad and \quad 0 \leq t_{cs} = \frac{\sqrt{|t^H \cdot \hat{t}|}}{\|t\| \cdot \|\hat{t}\|} \leq 1 \tag{2.25}$$

In the previous inequalities, r_{cs} and t_{cs} are used as performance measures for the RX and TX circuits responses' estimation, respectively. This inequality returns a value between 0 and 1, with 0 for the worst possible estimation and one for perfect estimation, which is obtained for $SINR = \infty$.

Deviation to Mean Ratio[3]

The ratio between the standard deviation and the mean can be used as a performance measure of the TX and RX circuits' responses. If the ratio is too big, it means the estimation method has not performed well. The digital base-band representation of the TX and RX circuits' complex responses form a cluster in the I-Q domain, as seen in Fig. 2.7 and Fig. 2.6. The blue arrow is the mean complex value, and the red and the green circles represent the clusters before and after calibration, respectively. The standard deviation is calculated as a 2-dimensional standard deviation, which equals the square root of the quadratic sum of the standard deviation in the I-axis and the standard deviation in the Q-axis, i.e. $\sigma_T = \sqrt{\sigma_I^2 + \sigma_Q^2}$. The equation for the calculation of the mean of a complex vector is given in Eq. 2.26.

$$\overline{R} = \overline{Real(R)} + i \cdot \overline{Imag(R)} \tag{2.26}$$

The estimated parameters are scaled by an unknown constant, but this does not affect the DMR performance tool, since this constant affects equally the standard deviation (σ) and the mean (μ). This is shown in Eq. 2.27 and Eq. 2.28.

$$Standard\ Deviation = \sigma_T = \sqrt{\frac{\sum (x-\mu)^2}{N}} \rightarrow \sqrt{\frac{\sum (c \cdot x - c \cdot \mu)^2}{N}} = c \cdot \sigma \tag{2.27}$$

$$Deviation\ to\ Mean\ Ratio\ (DMR) = \frac{c \cdot \sigma}{c \cdot \mu} = \frac{\sigma}{\mu} \tag{2.28}$$

The best estimation method is the one with the lowest deviation to mean ratio, given the same values of post-processing SNR and post-processing SIR.

2.3.4 Other Performance Measures

Since all the previously explained algorithms will be implemented in real systems, other performance measures must be taken into account, such as timing and memory consumption. These requirements may vary depending on the system

[3]This performance measure is proposed by the Master student.

in which the algorithms are implemented. Some systems may be very restricted by timing, and others may suffer from low computational power.

Timing and Memory Performance

Timing performance is a measure related to the time the system takes to run the estimation and calibration algorithms. Different algorithms take different times to run. If a system changes very fast, the calibration should be performed as fast as possible. In more stable systems, such timing restrictions may not be present. Further analysis on timing performance is out of the scope of the Master thesis.

Memory performance is a measure related to the amount of memory (e.g. RAM) required by the calibration algorithms to perform the necessary calculations. Since the calibration algorithms rely on the pseudo-inversion of one or more matrices, it will be important to ensure that the system is capable of performing such calculations. If the system has allocated a maximum memory for mathematical operations less than the required by the calibration algorithm, the operation will not be performed. Another procedure that uses less memory but more time to run would be needed in such case.

Overall Performance

A "cost-function" that contains all the performance measures can be defined in order to compare different methods not only in terms of accuracy but also in terms of timing and memory performance. To this end, the following terms may be defined: result performance (R_p), timing performance (T_p) and memory performance (M_p). In Eq. 2.29, α_1, α_2 and α_3 are used to scale each factor of the cost function, to give a different importance to each of the different parameters, depending on the system analyzed.

$$C_{total} = \alpha_1 \cdot R_p + \alpha_2 \cdot T_p + \alpha_3 \cdot M_p \tag{2.29}$$

2.3.5 Selected Tools

LLS and NLLS estimation methods have been chosen and applied for full measurements and neighbour measurements. CRLB was not used as a performance measure because the goal was to obtain a relative comparison between different methods, and hence an absolute comparison with respect to the best possible estimation method is not necessary. As it will be explained in Chapter 3, MSE and CSIN are measures that give information on the performance, but they do not provide enough relevant information when compared to the DMR. Hence, the DMR was determined to be the main performance measure for the Master thesis work.

Chapter 3

Simulation Study and Analysis of Results

This chapter contains a simulation study of some of the algorithms and methods explained in Chapter 2. These simulations are made considering an antenna array coupling matrix which may not be absolutely realistic. In any case, these simulations will serve as a reference case for the comparison of the different algorithms and estimators. The coupling matrix is assumed to be proportional to the distance between the elements, which is an assumption that may not hold for real systems. Hence, each particular system must be simulated in order to obtain its true performance. Two different calibration scenarios are considered, as explained in Section 2.1.3. The first one consists of a long-time calibration, to be performed when the system is deployed. The second one consists of a short-time calibration, performed cyclically and "on-the-go", in between system operation, i.e. when the system is transmitting and receiving data to and from user devices. For the first one, a big deviation in the TRX circuits' responses is assumed (refer to Fig. 3.1 for an example), and for the second one, the deviation is regarded as small (refer to Fig. 3.2 for an example).

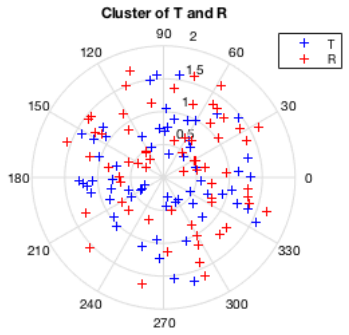

Figure 3.1: Big error cluster.

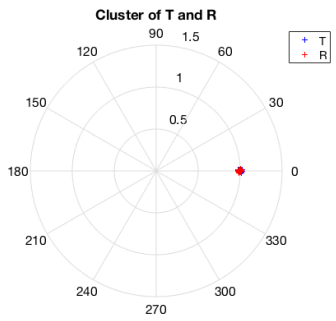

Figure 3.2: Small error cluster.

3.1 Calibration Algorithms

This section shows the performance of different combinations of measurement setups and estimation algorithms for their application to TRX circuits' calibration. All the following combinations were simulated and analyzed:

- LLS vs NLLS estimation methods.
- CSIN, DMR and MSE performance measures.
- Big initial error vs. small initial error.
- One iteration vs. two iterations of the calibration procedure.
- One or two or three levels of neighbours vs. full measurements.

Two iterations of the calibration procedure correspond to two sets of measurement plus calibration. This is: measurements are conducted, then calibration is applied. After that, measurements are conducted again, and a second calibration is applied. Since the measurements are conducted twice, there is a gain of 3dB in terms of equivalent post-processing SNR. The aim here is to check whether it is better to perform all the measurements together and make the calibration once, or it is better to conduct half the amount of measurements and calibrate, but twice. "Level 1" neighbours refers to the 8 neighbours directly surrounding an antenna element. For corner elements it refers to their three neighbour elements and, for the edge elements, it refers to the 5 neighbour elements. For "Level 2" neighbours, a total of 24 elements are considered (the corner and edge cases will have correspondingly fewer neighbours). The concept of levels of neighbours is illustrated in Fig. 3.3.

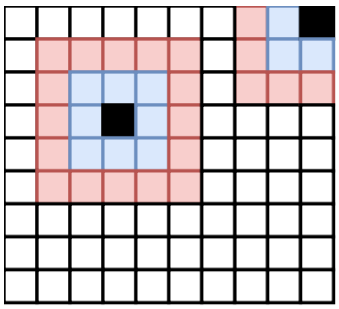

Figure 3.3: One level (blue) and two levels (blue + red) of neighbours for an inner and a corner element.

Simulations were conducted both with and without the knowledge and ignorance of interference. The known interference could be added to the antenna array coupling matrix to make an effective matrix of the form $H_{eff} = H + I$. Most of the simulations were done considering constant interference over the array and a few consider interference decaying faster than antenna array coupling gain over the array. All the simulations were done considering different post-processing SIR values. Infinite SIR means no interference over the antenna

array. Different values of post-processing SNR and SIR were tested, to check which values are required to obtain a certain system performance. Both values were defined with respect to 1. Hence, in order to translate from a value of "one" to the input power in the receive antenna ports, the coupling gain must be considered. This is usually done only with regards to the maximum coupling gain, which is -15 dB in this case. Then, the graphs will be exactly the same but with "real" post-processing SNR and SIR values 15 dB below the ones illustrated in the representations. Full knowledge of H_{eff} equals the case of knowledge of H with $SIR \rightarrow \infty$. Some other complementary information are given in Appendix A.2. It is well known that beamforming in an antenna array is achieved by changing the complex signals that excite each antenna element in the array. The effect of the phase component is more important than the effect of the amplitude component, with regards to the pointing direction. The TRX circuits' calibration algorithms simulated in this section have been found to be more effective in compensating for the error in the phase component than the amplitude component (as can be observed in Fig. B.1), and that is why these algorithms are well suited for the improvement of beamforming capabilities.

The unit "dBc" defines a relation between a reference signal and its leakage. A value of 0 dBc refers to the reference signal itself. An amount of -10 dBc refers to a tenth of the power of the reference signal.

3.1.1 No Interference Added

Some simulations were done considering $SIR \rightarrow \infty$. Simulations of full measurements using both LLS and NLLS estimation were performed. From Fig. 3.4 and Fig. 3.5, it can be concluded that, for a big initial error, it is best to use two iterations of the algorithm and, for a small initial error, the method is not so relevant.

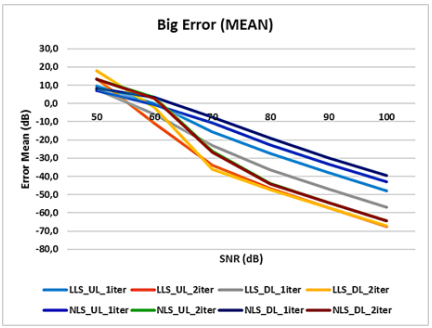

Figure 3.4: Error mean for big initial error.

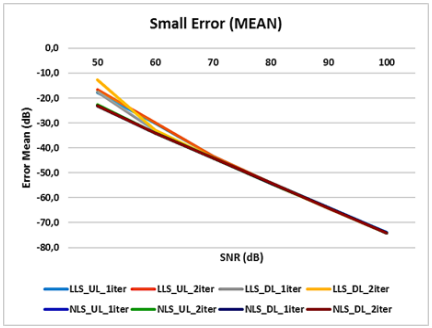

Figure 3.5: Error mean for small initial error.

3.1.2 Interference Constant over Antenna Array

Most of the simulations were done for a constant interference level over the antenna array. Different values of post-processing SNR and SIR were simulated for

every performance measure. Firstly, simulations of the CSIN, MSE and DMR performance measures are analyzed, in order to check whether or not any of these measures is redundant or useless. The post-processing SIR is defined with respect to the maximum value of antenna array coupling matrix. This means that, if the maximum antenna array coupling gain is, for instance, -15 dB, a post-processing SIR of 30 dB results in an interference level which is 45 dB below the signal level.

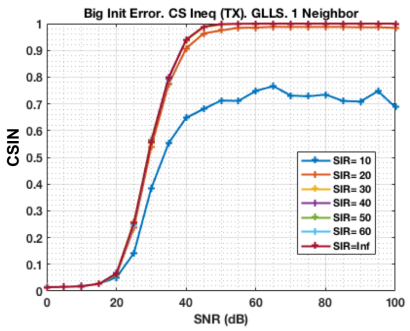

Figure 3.6: CSIN performance.

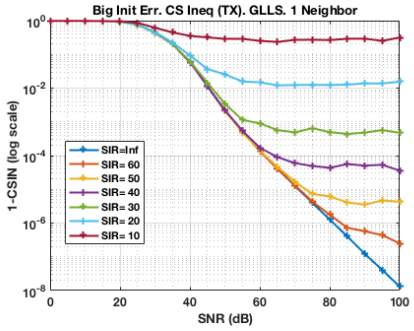

Figure 3.7: Modified CSIN performance.

In Fig. 3.6, one can observe the performance curves of the CSIN measure. The higher the post-processing SNR and SIR, the closer it is to the value of 1. By changing the representation to $(1 - CSIN)$ and forcing a semi-log scale, as in Fig. 3.7, one can separate the performance curves for high values of SIR and SNR. This representation looks very similar to that of the DRM, which is shown in Fig. 3.9. Thus, it does not make sense to use it. By observing the MSE representation in Fig. 3.8, and by comparing it against Fig. 3.9, one can see that the trend is similar to that of the DMR. Hence, MSE is also disregarded.

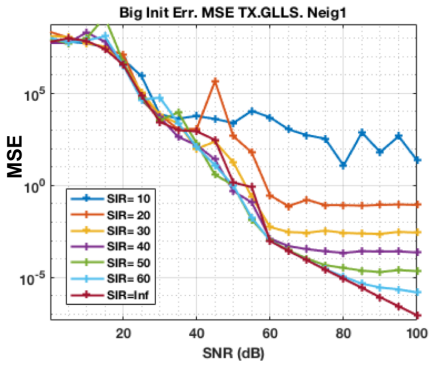

Figure 3.8: MSE performance with semilog-y scale.

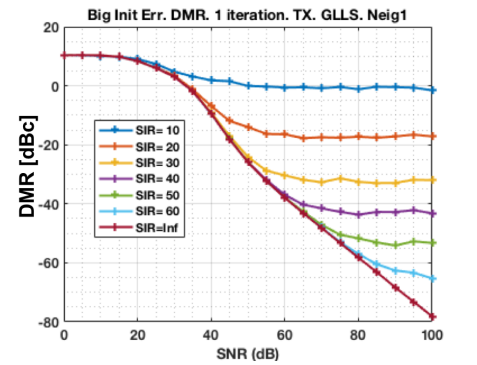

Figure 3.9: DMR performance, same scenario.

Big Initial Error

This section shows the performance of the TRX circuits' calibration when the initial error is big. Both TX and RX chains are considered. Besides, the performance of both the LLS and the NLLS estimation methods is simulated. One and two iterations of the calibration procedure are done as well. The estimation performance using one, two or three levels of neighbours, or full measurements is also compared. One must note that all the figures in this section show the DMR performance for the TX and/or RX chains.

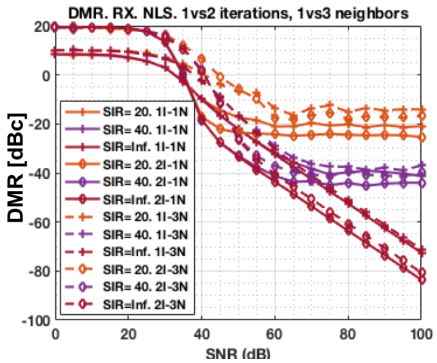

Figure 3.10: One vs. three neighbours (N), one vs. two iterations (I), NLLS estimation.

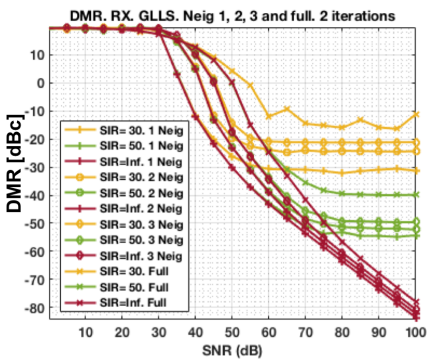

Figure 3.11: One, two or three neighbors and full, two iterations using LLS estimation.

From Fig. 3.10 and Fig. 3.11, which show the DMR performance of the RX chain, one can deduce that, the more the measurements used for the estimation of the TRX chains' responses, the worse is the performance. This is consistent with the results in Fig. 3.28 in Section 3.1.3, in terms of more measurements contributing to a poorer performance for the higher SNR range. As well as this, for the same number of measurements, it is better to iterate the calibration procedure twice. This is consistent with the results shown in Fig. 3.14 and Fig. 3.15.

In Fig. 3.12 and Fig. 3.13, which show the DMR performance for the RX vs. TX chain, a comparison of LLS and NLLS estimation methods can be found. The same conditions are applied as the previous figures: DMR performance measure, one neighbour measurement and two iterations of the calibration procedure. For lower values of post-processing SIR, the calibration using the NLLS estimation works better than the one using LLS estimation.

For LLS estimation and low values of the post-processing SIR, the estimation of the TX chains is worse than the estimation of the RX chains. This is because the first value of the TX chain estimation is forced to equal one in the LLS estimation, in order to avoid the all-zero solution. In Fig. 3.14 and Fig. 3.15, for the low post-processing SNR range, the performance is lower for two iterations than for one iteration of the calibration.

Analyzing Fig. 3.16 and Fig. 3.17, one can observe that, for high values of post-processing SIR and for one iteration of the calibration procedure, LLS estimation works better than NLLS estimation. The opposite happens for lower val-

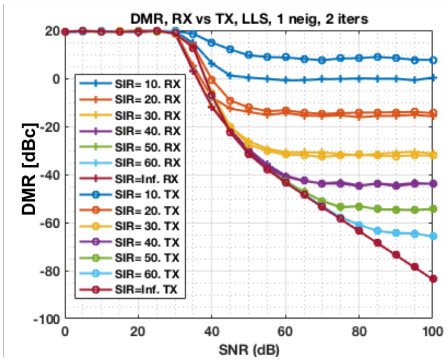

Figure 3.12: One neighbour and two iterations using LLS estimation.

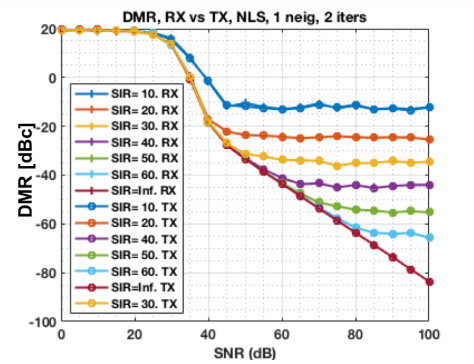

Figure 3.13: One neighbour and two iterations using NLLS estimation.

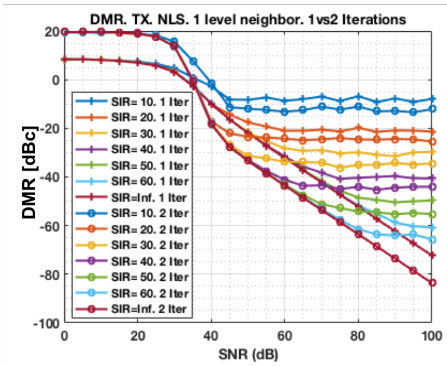

Figure 3.14: TX chain, one neighbour, one vs two iterations using NLLS estim.

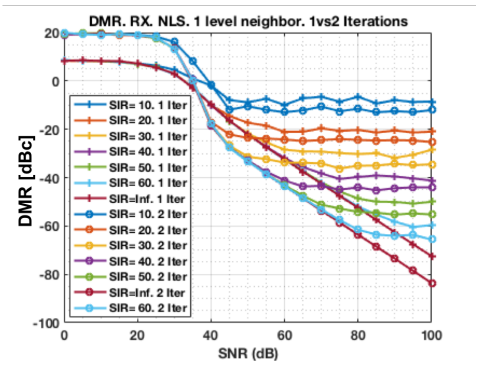

Figure 3.15: RX chain, one neighbour, one vs two iterations using NLLS estim.

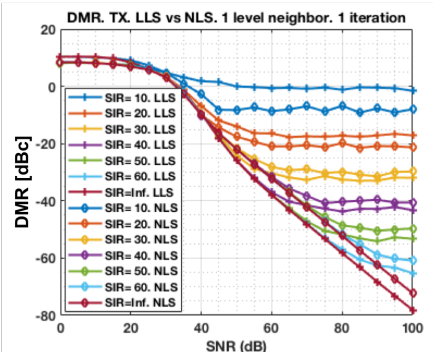

Figure 3.16: TX chain, one neighbour, LLS vs. NLLS, one iteration.

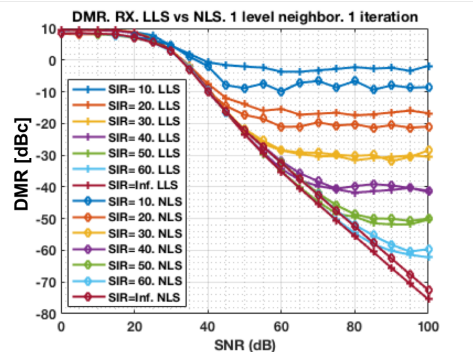

Figure 3.17: RX chain, one neighbour, LLS vs. NLLS, one iteration.

ues of post-processing SIR. The reason behind this may be that NLLS estimation has not converged. By increasing the number of iterations for NLLS estimation, this effect disappears. On the contrary, and since it is desirable to reduce the time the estimation takes, it is not recommendable to use NLLS estimation with a huge number of iterations. For low values of post-processing SNR, the NLLS estimation method performs better than LLS. By observing Fig. 3.18 and Fig. 3.19, it is easily concluded that two iterations of the calibration procedure give better results when using NLLS estimation than when using LLS estimation, for the low post-processing SIR range.

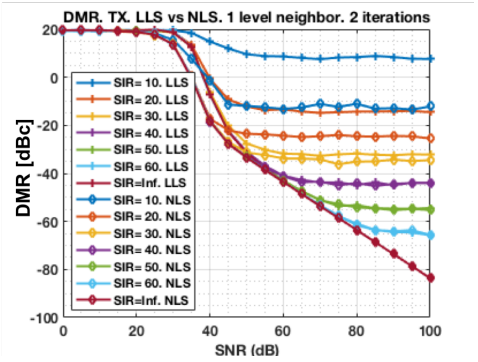

Figure 3.18: TX chain, one neighbour, LLS vs. NLLS, two iterations.

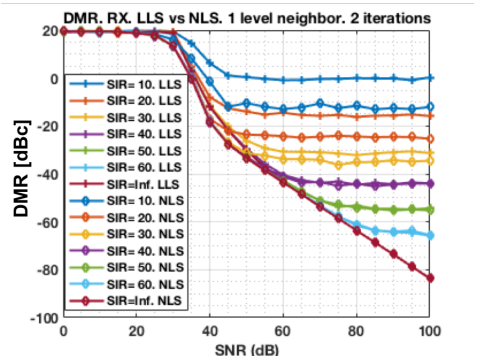

Figure 3.19: RX chain, one neighbour, LLS vs. NLLS, two iterations.

Several conclusions can be drawn:

- The fewer the number of neighbour measurements used for the estimation, the better are the results.
- Two iterations of the calibration procedure give the same or better performance than one iteration in the high post-processing SNR ranges, but worse for the low post-processing SNR ranges.
- For the NLLS estimation method, TX and RX chains' compensation gives the same performance.
- For low post-processing SIR ranges:
  - LLS estimation gives a better performance for RX estimation than for TX estimation.
  - LLS estimation gives a worse performance than NLLS estimation.
- For high post-processing SIR ranges:
  - LLS estimation and NLLS estimation gives the same performance for two iterations.
  - LLS estimation gives the best performance for one iteration.
  - TX and RX chains' compensation has the same performance for NLLS and LLS estimation.

Small Initial Error

The same simulations that were done in the previous section were done for this section, but considering a small initial error. From Fig. 3.20 and Fig. 3.21, one can deduce that, for a small initial error, two iterations of the calibration procedure performs worse than one iteration, in the case of low post-processing SIR values. The performance is the same for high post-processing SIR ranges. Besides, the performance is worse when a higher number of neighbour measurements are used for estimation purposes. All the observations are consistent with the conclusions drawn in the previous section for big initial error. One must note that the figures in this section show the DMR performance for the TX and/or RX chains.

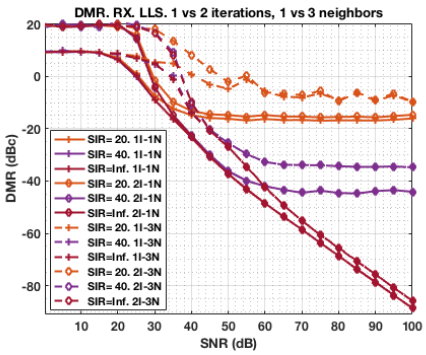

Figure 3.20: RX chain, one vs. three neighbours, LLS, one vs. two iterations.

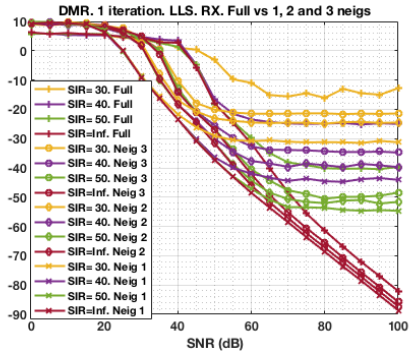

Figure 3.21: RX chain, one or two or three neighbours and full, LLS, one iteration.

Looking at Fig. 3.22 and Fig. 3.23, one can appreciate that NLLS estimation performs equally for TX and RX chains' estimation. For LLS estimation, the performance is equal across the different cases in the high post-processing SIR range. For the low post-processing SIR range, LLS estimation better estimates the RX chain than the TX chain. By looking at Figs. 3.24- 3.27, one can see that, for the high post-processing SIR range, both LLS and NLLS estimation give the same performance. For the low SIR range, LLS estimation has worse performance than NLLS estimation. The performance for two iterations is worse in the low SIR range in comparison to one iteration. This trend is consistent with what is shown in Fig. 3.20. It can be seen that the behaviour of these estimation methods for a small initial error is very similar to the one with a big initial error (i.e. big deviation) in the TRX chains' responses. It is our goal (as will be explained in the following chapter) to get a deviation to mean ratio (after calibration) of around -45 dBc. If an internal interference level of -45 dBc (i.e. SIR=45 dB) is present, a post-processing SNR value of 70 dB will lead to a performance of around -50 dBc, both for one or two iterations of the calibration procedure, using one level of neighbors. Thus, for a small initial error, it is better to use LLS estimation and one iteration of the calibration procedure, if the interference level is small enough. If the interference level is big, it is better to use NLLS estimation and one iteration. Two iterations do not improve the performance for a small initial error.

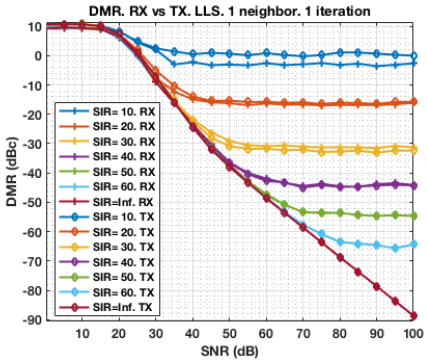

Figure 3.22: RX vs TX chain , one neighbour, LLS, one iteration.

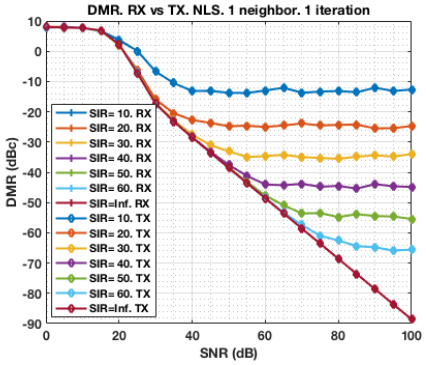

Figure 3.23: RX vs TX chain, one neighbour, NLLS, one iteration.

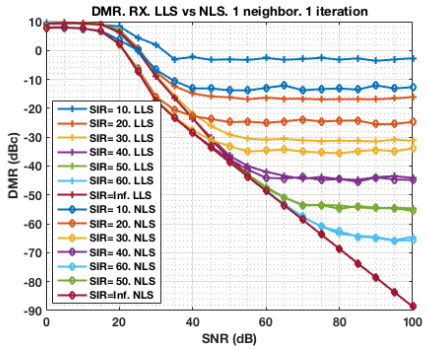

Figure 3.24: RX chain, one neighbour, LLS vs. NLLS, one iteration.

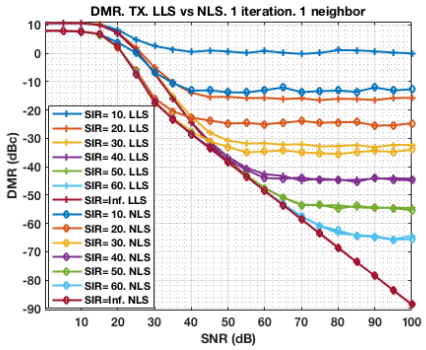

Figure 3.25: TX, one neighbour, LLS vs. NLLS, one iteration.

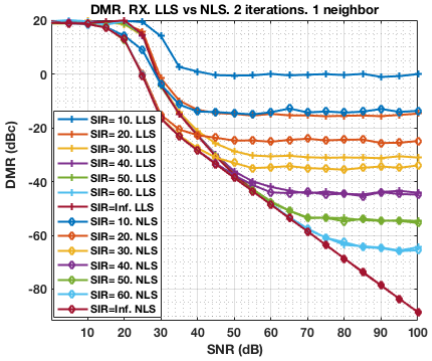

Figure 3.26: RX chain, one neighbour, LLS vs. NLLS, two iterations.

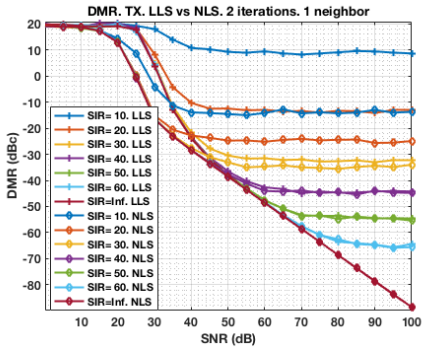

Figure 3.27: TX chain, one neighbour, LLS vs. NLLS, two iterations.

3.1.3 Interference Varying over Array Aperture

The effect of an interference which varies in power over the array aperture is analyzed here. NLLS estimation was used, together with DMR as the performance measure. A small initial error is considered, since the results for a big initial error are similar. In Figs. 3.28- 3.30, the legend has the following structure: NX_I-YY, where X refers to the level of neighbours and YY refers to the interference value with respect to the maximum coupling gain.

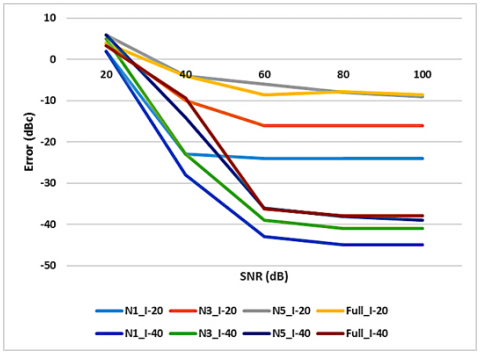

Figure 3.28: Constant Interference over array elements.

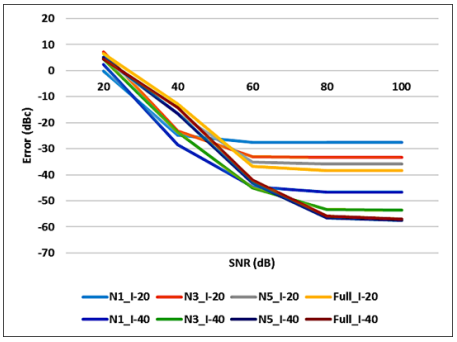

Figure 3.29: Decay in interference equal to coupling gain.

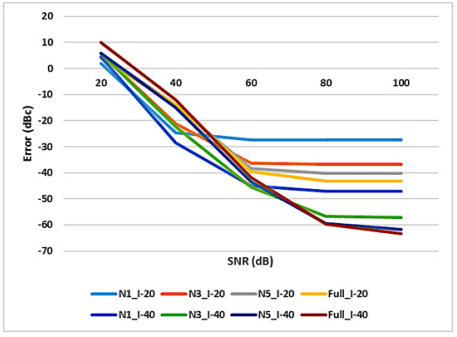

Figure 3.30: Interference decaying faster than coupling gain.

Measurements with an unknown interference result in a lower performance of the calibration algorithm (as compared to known interference or no interference). This is due to the deviation to mean ratio not being reduced with an increasing value of the post-processing SNR, given a concrete value of the post-processing SIR. With a constant interference over the array aperture, estimation with less neighbours performs better. For neighbouring antenna elements that are further away, the ratio between the antenna coupling gain and the unknown interference decreases, resulting in lower quality measurements. When the interference decays equally to or faster than the coupling gain between the antennas in the array, it is better to use fewer neighbours in the low post-processing SNR

region. In the high SNR region, it is better to use more elements.

3.2 Antenna Coupling Matrix Estimator

This estimator is based on the use of two kind of measurements, each of them performed in different time instants thus with uncorrelated noise and interference effects. The first measurement consists of the acquisition of an electromagnetic plane wave sent by the probe antenna and received by the DUT. The second measurement consists of self-measurements in the DUT, which are the same as the ones performed in the previous section. Different values of post-processing SNR must be simulated in each of the involved measurements. Since two estimators were proposed, both of them were tested. The first one worked, but the second one did not. Therefore, only the results from the first estimator are shown. For the self-measurements simulations, a reciprocal interference was assumed. More simulations considering a non-reciprocal interference can be done, in order to find out the effect of the interference on the performance of the estimator.

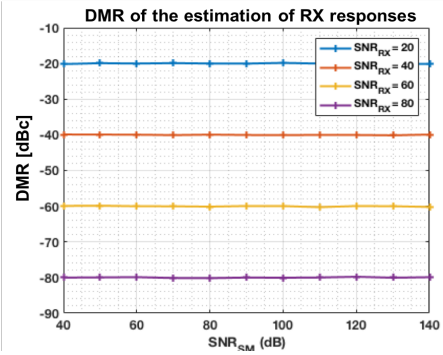

Figure 3.31: DMR estimation of RX responses.

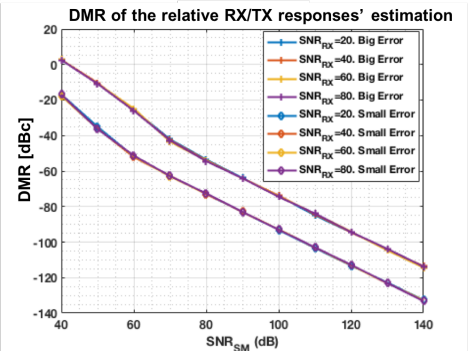

Figure 3.32: Relative C = RX/TX responses' estimation.

The estimation of the antenna array coupling matrix is done before any previous TRX chains' calibration. Therefore, any initial state can be expected. Thus, the deviation of the TRX chains' responses cannot be assumed to be small. In the following figures, SNR_{RX} refers to the SNR at each receive antenna port for the plane wave acquisition. SNR_{SM} refers to the SNR in each RX antenna port for the self-measurements procedure. This SNR is different from the one shown in the previous section. Fig. 3.31 shows the DMR of the RX chains' responses estimation. The SNR in the self-measurements does not affect the performance of the RX chain responses estimations, since both procedures are independent of each other. As well as this, the DMR of the RX chain responses equals the inverse of the SNR of the plane wave acquisition. In Fig. 3.32, the DMR of the estimation of the relative receive to transmit (RX/TX) chain responses is shown.

Fig. 3.33 shows the DMR of the normalization of the estimated antenna array coupling matrix divided by the actual antenna array coupling matrix (i.e. H_{est}/H). As can be seen in Fig. 3.33, big initial error and small initial error result

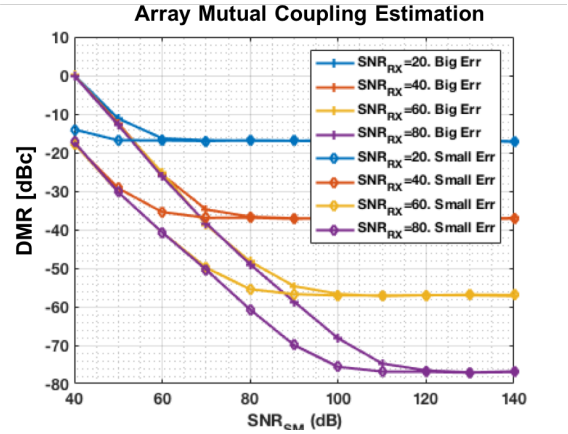

Figure 3.33: DMR of array mutual coupling estimation for reciprocal interference. Big vs. small initial error.

in the same performance for the high post-processing SNR range. For low SNR values, the estimation is better with a small initial error. The noise present in the estimation of the RX chains' responses will act as an interference in the antenna array coupling matrix estimation, since both measurements are independent. The full signal model for the self-measurements is shown below, where μ_i^{RX} is the noise present in the RX chains responses' estimation.

$$Y_{ij}^{SM} = (r_i + \mu_i^{RX}) \cdot h_{ij} \cdot t_j + n_{ij}^{SM} \tag{3.1}$$

It is important to find a balance between the SNR in the plane wave measurements and the SNR in the self-measurements, since the performance of the estimation saturates for very high SNR values in the plane wave acquisition. The y-axis in Fig. 3.33 shows the power of the interference that will be inherently present when the estimated antenna array matrix is used for TRX calibration purposes. Reciprocal interference was considered in the self-measurements of these simulations. It is proposed, as future work, to consider non-reciprocal interferencein the simulations, in order to check its effect on the performance of the antenna array coupling matrix estimator.

Chapter 4

Radio Module Considerations and Measurements Setup

Ideas, concepts and simulations are important, but it is mandatory to test some of these ideas and simulations in a practical setup, to confirm their validity in a real environment. After introducing and explaining the calibration and coupling matrix estimation algorithms, it is time to detail their possibilities and limitations in an Ericsson radio module. As well as this, some measurements must be conducted in a testbed in order to validate the algorithms and estimators.

4.1 Radio Module Considerations

An overview of the radio module to be used as a DUT is illustrated in this section, with its considerations and design features and capabilities. Limitations in the system are also explained.

4.1.1 System Overview

In this section, a brief description of the system is done, in order to clarify how it works in a real environment. This system is a radio access module, containing a total of 64 active antenna elements and 40 surrounding idle elements. The antenna array is shown in Fig. 4.1. The aim of these 40 idle elements is to obtain a uniform impedance over the array aperture. The system is a radio module/ASIC system composed of 4 TRX blocks, connected to 4 antenna modules. Each antenna module supports two polarizations.

Each TRX block consists of two 16-element IF TRX chains, one for each polarization. Each antenna module consists of four RFICs and a package with 64 integrated dual polarized patch antenna elements. Each RFIC has two independent radio groups with 8 TX/RX chains in each group and in each polarization.

The arrangement in the radio module/ASIC is illustrated in Fig. 4.2, where crosses represent the antenna elements (one must note the numbering is not correct in this image). The antenna element placement, when it is seen from above, is given on Table 4.1. An schematic of the antenna module architecture and the RF IC architecture can be found in [15].

Limitations in the Availability of Self-measurements

The system is limited in terms of available self-measurements, since there are radio groups that can be configured to only transmit or only receive. If one antenna element in one radio group is transmitting or receiving, none of the other 7 elements in the same radio group can be configured to receive or to transmit, respectively. When one element is transmitting, no other element in the same radio group can receive. Physical connections are the limiting factor for the self-measurements capabilities.

Some TX-to-RX paths are not available because they are connected to the same ADC. Regarding the self-measurements, the elements with coupling gain below -30 dB should be considered very carefully, and the ones with coupling gain below -40 dB should be discarded. The limitations in self-measurements capabilities caused by hardware connections limits not only the TRX circuits' calibration but also the antenna array coupling matrix estimation. Regarding the TRX circuits' calibration, there is access to a limited number of self-measurements, which can result in a decreased performance with regards to systems without any hardware constraint.

The simulated coupling matrix from the antenna array was provided, and it is illustrated in Fig. 4.3. The upper-left quadrant contains the horizontal to horizontal polarization coupling gain, the bottom-right quadrant contains the vertical to vertical polarization coupling gain, the upper-right quadrant and the bottom-left quadrant contain the cross-polarizations coupling gains. The element S_{ij} in the matrix refers to the portion of power that is sent from the antenna element j and received in the antenna element i.

Measurements from elements in one RFIC to elements in another RFIC can be performed. Cross-polarization measurements can be performed as well. The decision was to make the measurements inside one polarization, in order to simplify the complexity of the measurement setup. The mean of the coupling gains computed over all the antenna elements is illustrated in Fig. 4.4. It is computed by averaging the coupling gains from each element to the others, over the entire array. Taking into account the connections' constraints and a minimum acceptable coupling gain of -40 dB, the measurement sets can be defined.

RC	**0**	**1**	**2**	**3**	**4**	**5**	**6**	**7**
0	0-15	0-14	0-6	0-7	1-15	1-14	1-6	1-7
1	0-13	0-12	0-4	0-5	1-13	1-12	1-4	1-5
2	0-10	0-11	0-3	0-2	1-10	1-11	1-3	1-2
3	0-8	0-9	0-1	0-0	1-8	1-9	1-1	1-0
4	3-0	3-1	3-9	3-8	2-0	2-1	2-9	2-8
5	3-2	3-3	3-11	3-10	2-2	2-3	2-11	2-10
6	3-5	3-4	3-12	3-13	2-5	2-4	2-12	2-13
7	3-7	3-6	3-14	3-15	2-7	2-6	2-14	2-15

Table 4.1: Antenna element placement as seen from above i.e. looking down at the antenna array.

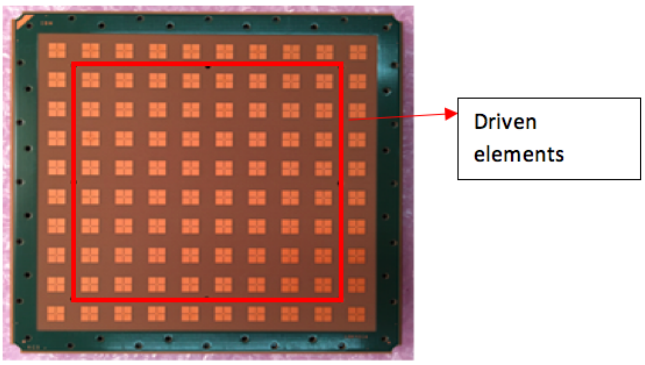

Figure 4.1: Antenna array front view, showing both driven and idle elements.

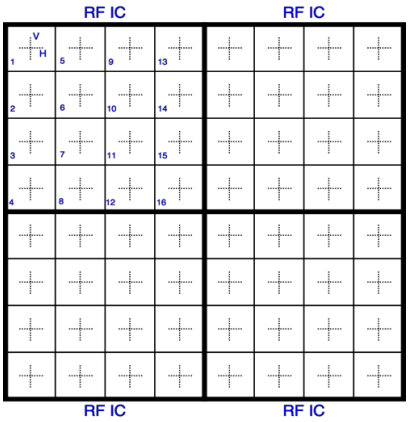

Figure 4.2: Antenna elements arranged over 4 RFICs.

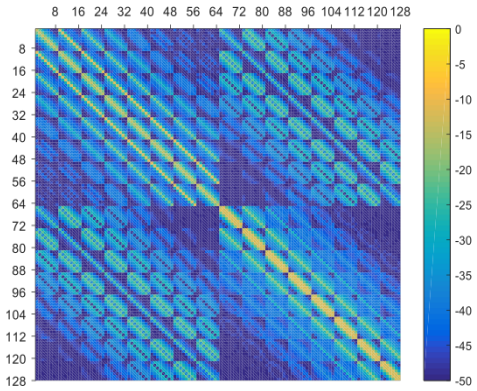

Figure 4.3: Simulated coupling matrix.

The values illustrated in Fig. 4.4 are of a high interest. These values are used as a "rule-of-thumb" to define neighbour elements and power parameters for TRX circuits' calibration in real systems developed by Ericsson, where a similar antenna array is used.

Interference inside RFICs

The circuits' interference inside each RF IC in the radio module must be considered. Internal information in the company stated the internal leakage inside a RFIC to be around -45 dBc between antenna elements. The internal leakage between RFICs is around -90 dBc. It was agreed that this internal leakage should be modeled as an uniformly distributed random variable. In Section 2.2, it was stated that the antenna array coupling matrix estimation method developed internally in Ericsson could eliminate the internal leakage effect, under certain con-

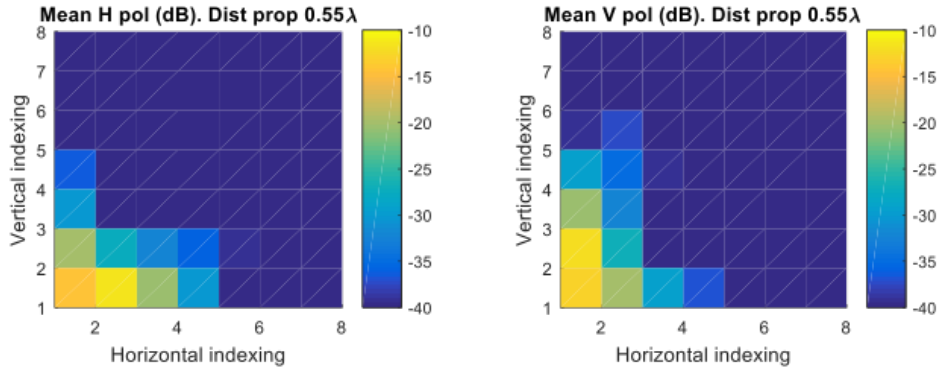

Figure 4.4: Mean coupling over all antenna array.

straints. If these constraints do not hold, the internal leakage must be taken as an extra source of interference.

4.1.2 Other System Considerations

Timing requirements

TRX circuits' calibration must be performed in the shortest amount of time possible. This was explained in Section 2.1.3, but in this section we are applying this requirement to the radio module made available for the project. The system would stop working for a short time when performing the self-measurements. One advantage is that the estimation of the TRX circuits' responses and the data transmission/reception can run in parallel in a Field Programmable Gate Array (FPGA). Hence, the only time-limiting factor is the time the system takes to make the self-measurements. In Fig. 4.5, a timing scheme can be found.

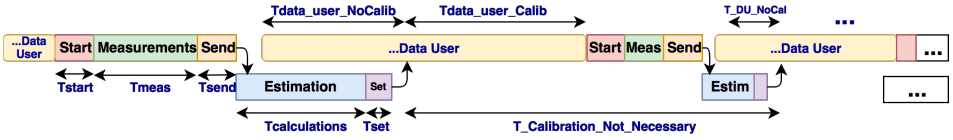

Figure 4.5: Timing requirements for the calibration procedure.

- T_{start}: initial time to start the self-measurements.
- T_{meas}: time to perform the self-measurements. This depends on the integration time.
- T_{send}: time to send the raw measurements for estimation and calibration.
- $T_{calculations}$: time to perform the estimation.
- T_{set}: time to calibrate the TRX circuits' responses.

- $T_{data-user-NoCalib}$: period of time during which calibration has not been applied and data from users is transmitted and received.
- $T_{data-user-Calib}$: period of time when data from users is transmitted and received after calibration is applied.
- $T_{Calibration-Not-Necessary}$: time when no calibration is necessary.

The aim is to minimize the time periods T_{start}, T_{meas} and T_{send}, without critically reducing the performance of the estimation, since this minimizes the total calibration time, thus increasing the overall efficiency of the system.

Power Requirements

The power level of the test signals used in the self-measurements must be defined as well. Each receiver in the radio module will accept a certain maximum input power (let's refer to it as XX dBm) without running into compression. The maximum transmit power, which will not run the receiver into compression, must be selected with regards to the maximum coupling gain in the antenna array. The provided maximum antenna array coupling gain in the radio module is -11.6 dB. A basic link budget calculation states:

$$P_{TX} = P_{RX} - max(H) = XX\ dBm + 11.6\ dB. \tag{4.1}$$

By considering N_0 to be the noise spectral density, NF to be the noise figure of each receiver, and BW_{dB} the bandwidth of the signal in decibels, one can derive the noise level in the system as:

$$N_{PW} = N_0 + NF + BW_{dB} = -174\ dBm + 11\ dB + 86\ dB = -77\ dBm. \tag{4.2}$$

The SNR of the self-measurement related to the strongest coupling gain can be calculated, by using Eq. 4.2, as:

$$SNR\ (dB) = max(P_{RX}) - N_{PW} = XX - (-77)\ dB. \tag{4.3}$$

If a certain performance is desired and the SNR level for one cycle of one measurement does not bring that performance, a post-processing SNR must be obtain by averaging over several cycles of the same measurement. The number of minimum cycles is:

$$N_{cycles} = \lceil 10^{\frac{SNR_{desired} - SNR_{1cycle}}{10}} \rceil. \tag{4.4}$$

Similar calculations can be made for the measurement related to the plane wave acquisition, since these calculations are related to the power levels in the self-measurements.

4.2 Simulations using Radio Module Features

A few simulations have been made in this section, by taking radio module features into consideration. The aim of these simulations is to get an idea of the post-processing SNR and SIR values that are required to achieve a certain performance in the system, before performing the measurements in the testbed.

4.2.1 TRX Circuits' Calibration

In these simulations, only the self-measurements with a coupling gain higher than -40 dB were considered. As well as this, post-processing SNR and SIR values were defined with respect to the power transmitted by the TX elements. If the definition must be made with regard to the maximum received power in an antenna port, the maximum coupling gain (11.6 dB) must be subtracted from the SNR and SIR values. Thus, if a performance value of -40 dBc is obtained for $SNR = 40$ dB and $SIR = 50$ dB, the SNR and the SIR in the antenna port for the maximum coupling gain will be $SNR = 28.4$ dB and $SIR = 38.4$ dB. In this section, all the figures show the DMR performance of the TRX circuits' calibration.

Big Initial Error

In this part, the performance of the TRX circuits' calibration, with a big initial error in the circuits' responses, is calculated. In Fig. 4.6 and Fig. 4.7, one can see a comparison between one and two iterations of the calibration calculation, by estimating the RX circuits' responses using both LLS and NLLS estimation.

Two iterations of the calibration procedure work better than one iteration, for high values of post-processing SIR, and worse for low values, which is consistent with the conclusions drawn in Section 3.1.2. By observing Figs. 4.8-4.11, one can conclude that one iteration of the calibration procedure performs better with LLS estimation, for high values of the SIR. On the contrary, NLLS estimation works better for low values of SIR. For two iterations, NLLS estimation works better in the low post-processing SIR range. There is no difference in performance for the high SIR range. For the low post-processing SNR range, two iterations perform worse than one iteration. All these conclusions are consistent with the simulations of the generic signal model used in Chapter 3.

Small Initial Error

In this part, the performance of TRX circuits' calibration for the radio module, with a small initial error in the TRX chains' responses, is analyzed. In Fig. 4.12 and Fig. 4.13, one can observe that two iterations perform better than one iteration for high values of post-processing SIR, and worse for low values. By observing Figs. 4.14-4.17, one can see that one iteration using LLS estimation performs better in the high SIR range than in the low SIR range. The opposite happens for NLLS estimation. For two iterations, NLLS estimation is better for low SIR values and equal in performance for high values. All these conclusions are, again, consistent with Section 3.1.2.

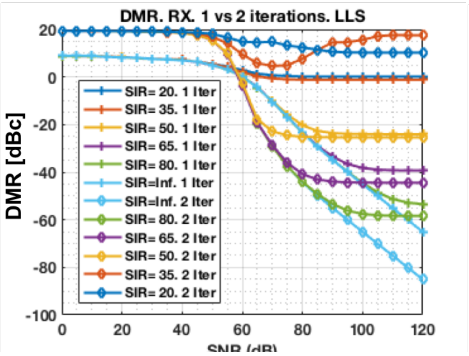

Figure 4.6: RX chain, 1 vs. 2 iterations, LLS estimation. Big error.

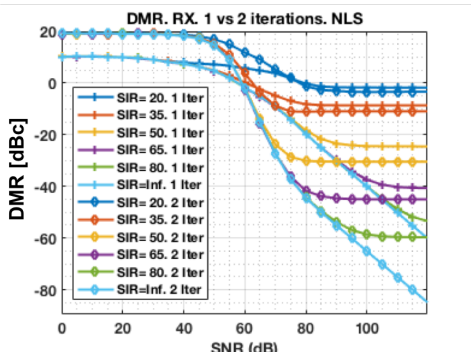

Figure 4.7: RX chain, 1 vs. 2 iterations, NLLS estimation. Big error.

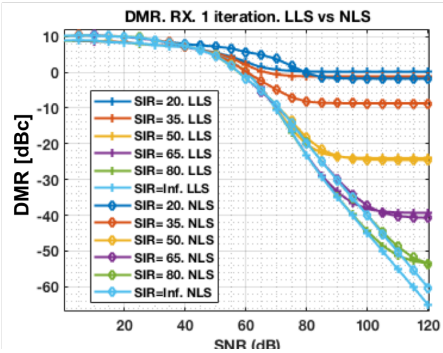

Figure 4.8: LLS vs. NLLS with one iteration (RX chain). Big error.

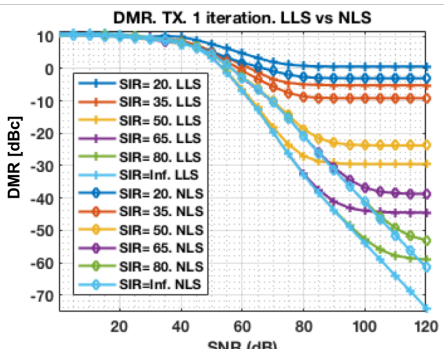

Figure 4.9: LLS vs. NLLS with one iteration (TX chain). Big error.

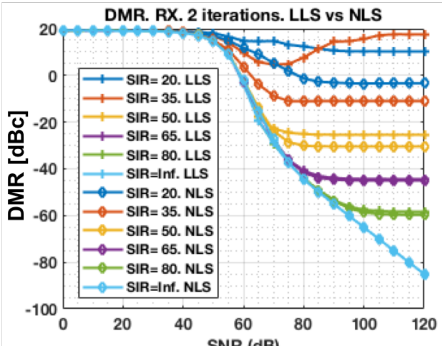

Figure 4.10: LLS vs. NLLS with two iterations (RX chain). Big error.

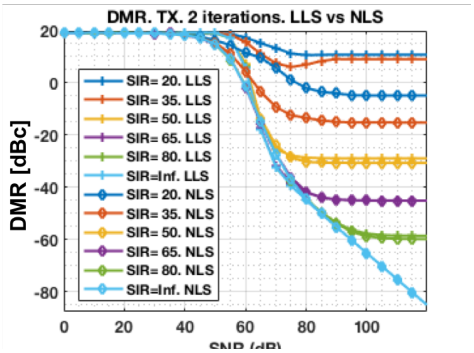

Figure 4.11: LLS vs. NLLS with two iterations (TX chain). Big error.

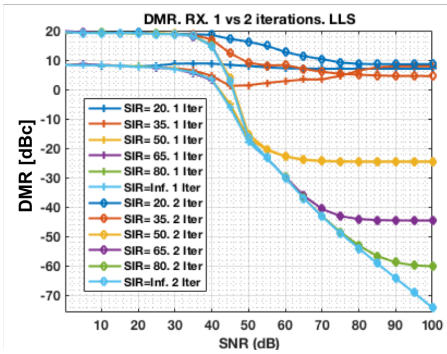

Figure 4.12: RX chain, 1 vs. 2 iterations, LLS estimation. Small Error.

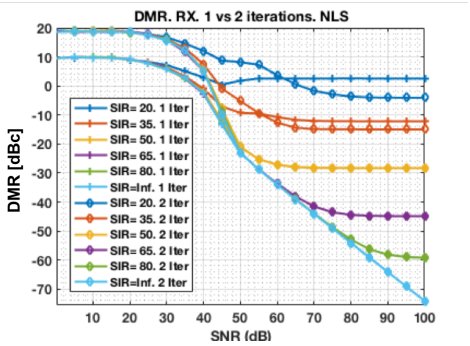

Figure 4.13: RX chain, 1 vs. 2 iterations, NLLS estimation. Small Error.

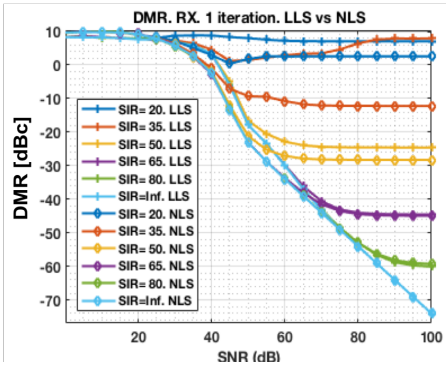

Figure 4.14: LLS vs. NLLS performing one iteration (RX). Small Error.

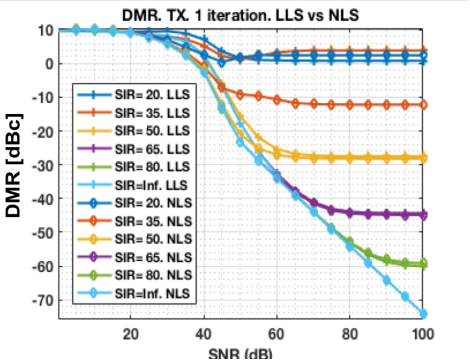

Figure 4.15: LLS vs. NLLS with one iteration (TX). Small Error.

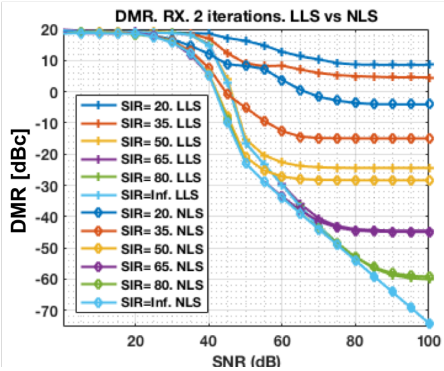

Figure 4.16: LLS vs. NLLS with two iterations (RX chain). Small Error.

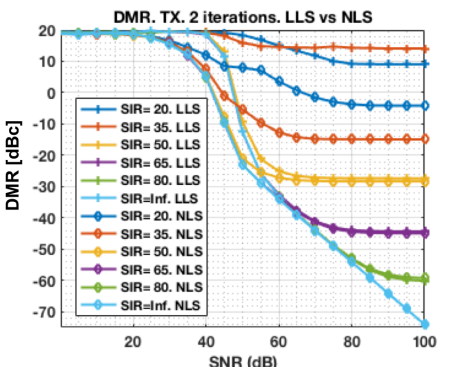

Figure 4.17: LLS vs. NLLS with two iterations (TX chain). Small Error.

Conclusions

Some specific simulations are needed for each particular system in case an specific performance is sought. For instance, in our case, a performance of -45 dBc is desired. There are two ways to achieve this:

- One iteration $\rightarrow SNR = 110; dB$ and $SIR = 70; dB$, either LLS or NLLS.
- Two iterations $\rightarrow SNR = 90; dB$ and $SIR = 65; dB$, either LLS or NLLS.

For the previous values, it seems that the initial performance requirements may need to be relaxed, but more simulations are needed to confirm this. It is expected that, by using the least number of the strongest neighbour elements, the results would be better. This aspect is left for future work.

4.2.2 Antenna Coupling Matrix Estimator

In this section, the performance of the antenna array coupling matrix estimator for the radio module is simulated. Two noisy calculations must be done. The first noisy measurement is related to the plane wave measurement acquisition from the horn antenna to the radio module and the second relates to the self-measurements. Reciprocal interference was assumed in the self-measurement simulations.

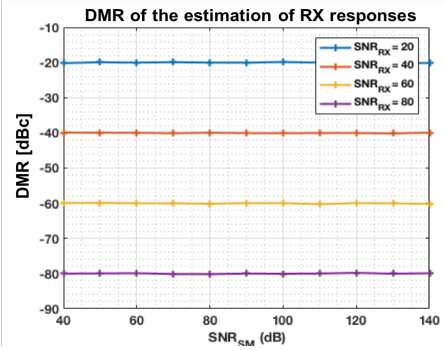

Figure 4.18: DMR performance for estimation of RX chains.

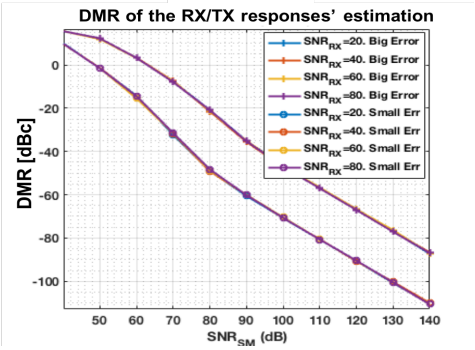

Figure 4.19: Relative C = RX/TX responses' estimation.

By looking at Fig. 4.18 and Fig. 4.19, one can see that the noise in the plane wave acquisition (SNR_{RX}) directly affects the estimation of the RX circuits' responses, but does not affect the relative RX to TX responses. The opposite trend happens for the noise in the self-measurements (SNR_{SM}). For a small initial error, the estimation of the relative RX to TX chain responses is better than for a big initial error. All these observations are consistent with the results in Section 3.2.

Fig. 4.20 shows that, for high values of post-processing SNR_{SM}, the estimation algorithm gives the same performance, both for a small and a big initial error. For low values of post-processing SNR_{SM}, the estimation is better for a small initial error than for a big initial error. The noise present in the estimated

RX circuits' responses will act as an interference in the antenna array coupling matrix estimation, thus limiting the estimation performance. As well as this, Fig. 4.20 shows that an increase in SNR_{SM} may not bring any improvement in the estimation performance, for certain values of SNR_{SM}.

The behavior obtained by using the radio module parameters shares the same trends as the behavior obtained using the generic signal model. This confirms that the general signal model is good enough to be considered as a reference case for estimation performance.

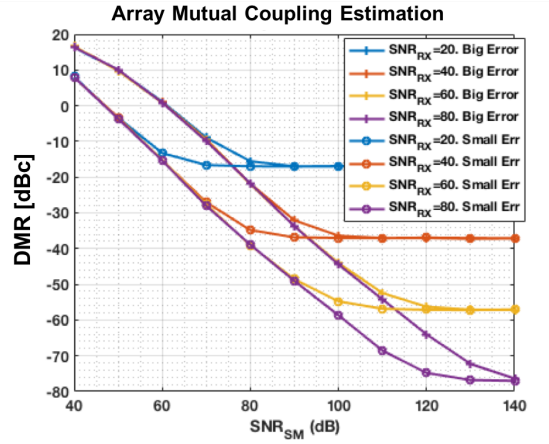

Figure 4.20: DMR of array mutual coupling estimation for reciprocal interference. Big vs. small initial error.

4.3 Test Signal

This system is intended to work in the 28 GHz band, utilizing a maximum bandwidth of 800 MHz. Thus, a test signal with a bandwidth of 800 MHz, centered at 28 GHz must be defined. The aim is to send a multi-tone test signal with constant amplitude in the frequency domain, but with different phase values in each spectral component. The aim of using different phase values is to reduce the peak to average power ratio (PAPR) in the time domain, in order to increase the efficiency of the RF circuitry. This signal can be defined by using the IFFT operation. The train of deltas in frequency (i.e. multi-tone signal) will have the structure shown in Fig. 4.21, with each tone having a certain phase value.

To select the proper phase value in each tone, a brute-force search was performed, using MATLAB. In Fig.4.22, one can find the trend of the power-to-average-power ratio (PAPR), given different combinations of signal constellation, number of tones over the bandwidth and number of iterations for the brute force search. The results in this figure will be used as a reference to define the test signal to be used in TRX circuits' calibration of real systems developed by Ericsson. The mathematical formulation of this problem is given in Eq. 4.5, where $Tones(f, \phi)$

refers to the mathematical formulation of the tones. Due to computational limitations, we had to limit the number of phases and tones that were tested. For k tones in frequency and N phases, there is a total of N^k combinations. For high values of N and k, the computation time required by the simulation is not feasible for this project.

$$s(t,\phi) = IFFT_f(Tones(f,\phi)) \quad and \quad \hat{\phi} = arg\min_{\phi}\left(\frac{max|s(t,\phi)|}{\sqrt{\|s(t,\phi)\|_2}}\right) \tag{4.5}$$

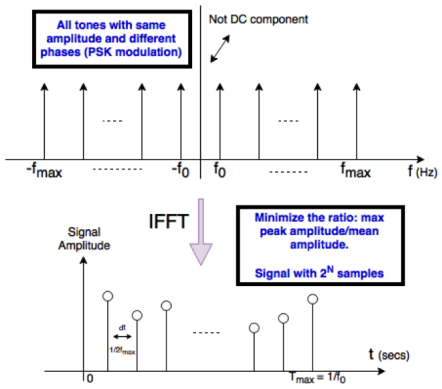

Figure 4.21: Test signal generation.

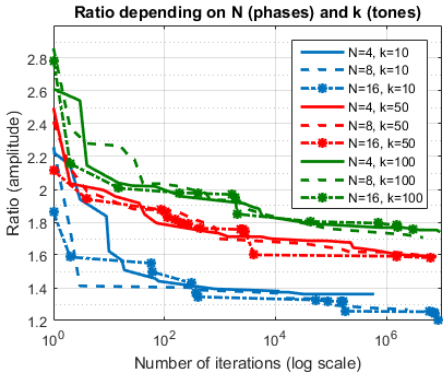

Figure 4.22: PAPR for different simulation sets.

Initially, the idea was to use a sequence generated from a signal created by using the previous explained above, but a better method was found. In other Ericsson premises, some calibration measurements were done using a method based on the cross-correlation of two signals. The method correlates a signal with a BW of ≈100 MHz with the same signal but scaled and delayed by the path between the TX and RX. The correlation returns a signal with a BW of ≈100 Hz, from which one can extract the delay and complex scaling factor. This method has been shown to work quite well even under low SNR conditions, since it brings a post-processing SNR gain of 60 dB. The only drawback is that it can only measure one frequency tone at a time.

4.4 Testbed Features and Measurements Strategy

4.4.1 Testbed Features

A description of the testbed features, its signal levels and frequencies, and its physical connections is provided in this section. Some pictures of the testbed are shown in Fig. 4.23. This setup is composed of a lab PC, a radio module/ASIC, a TRX board, a power supply, a horn antenna, some RF components and one LAN switch (apart from some measurement equipment that was already in place). The

connection to the LAN switch allows for higher scalability and adaptability. The schematic of the testbed is provided in Fig. C.1. In Table C.1, one can find a complete list of the components used in the testbed.

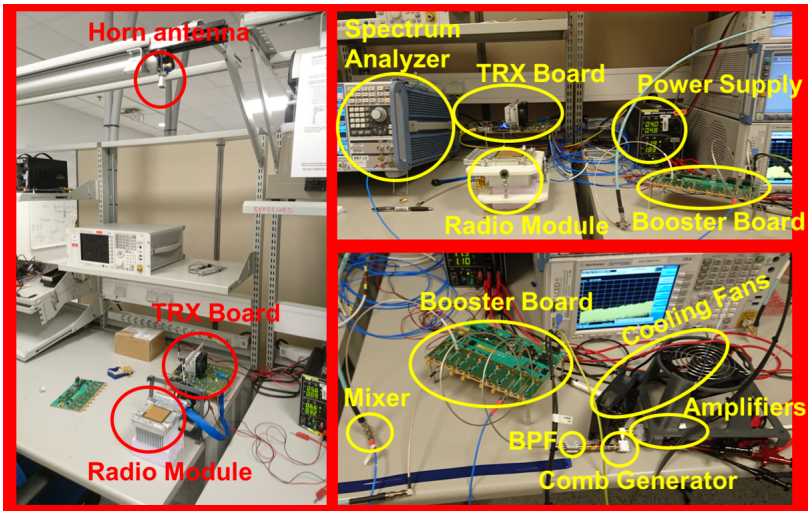

Figure 4.23: Pictures of the testbed setup at Ericsson's Laboratory.

4.4.2 Signal Levels and Frequencies

A detailed description of the signal levels and frequencies of the testbed system is given in this section. After the measurements are performed with the testbed in a lab environment, the same measurements must be performed in an anechoic chamber, since the lab environment suffers from the presence of interference and the anechoic chamber (ideally) do not. There are three main parts in the measurement system:

- External LO path (one way, from TRX board to mixer).
- IF and RF external paths (two ways, from horn antenna to TRX board and vice-versa).
- Over-the-air (OTA) propagation path.

External LO Path

This is a one-way path, from TRX board to mixer, and it is in charge of generating a high frequency LO signal to be used in the mixer. The aim of that signal is to up/down-convert the IF/RF signals sent to/from the horn antenna from/to the TRX board. The LO signal path schematic is illustrated in Fig. 4.24.

This external path starts in the TRX board, which generates a pure tone (LO signal) at 5.17 GHz. The power level of this tone can be set between -3 and 5 dBm. This signal is amplified by two power amplifiers, and the amplified signal power

can be up to 18 dBm. The amplifiers must be powered with a +7V (obligatory) and a -0.3V (optional, but improves performance) DC inputs. The amplified signal enters a comb generator which produces integer product tones of the input signal as $f_{out} = n \cdot f_{in}$ with $n \in \mathbb{N}$, i.e. 5.17 GHz, 10.34 GHz, 15.51 GHz, 20.68 GHz, 25.85 GHz, 31.02 GHz, 36.19 GHz, 41.36 GHz, etc. Since it is a passive element, the power of each integer product is reduced with respect to the input power, with a higher reduction the higher the integer product. The signal composed of the integer tones enters a band-pass filter (BPF) centered at 32 GHz, with a bandwidth of 10 GHz. Then, only the 5th, 6th and 7th integer products get out of the BPF with a substantial power level. The filtered signal feeds the booster board, which amplifies the 31 GHz tone. The booster board can also be used to amplify the modulated 28 GHz signal.

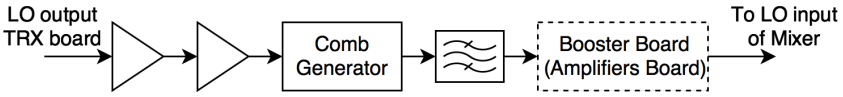

Figure 4.24: LO path. From TRX board to mixer (one way).

Using the information present in Appendix C.1, one can calculate the full response of this path. It is expected to create the following tones (weakest ones are not considered), with the following power levels:

- At 25.85 GHz $\rightarrow$ PW $\approx$ -57 dBm.
- At 31 GHz $\rightarrow$ PW $\approx$ **-18 dBm**.
- At 36.2 GHz $\rightarrow$ PW $\approx$ -25 dBm.
- At 41.4 GHz $\rightarrow$ PW $\approx$ -60 dBm.

The strongest tone entering the mixer is the one at 31 GHz, but there is another tone that must be accounted for, which is the one at 36.2 GHz. These two tones can result in mixed spurious signals. The booster board is expected to amplify the tone at 31 GHz but also the tone at 36 GHz (with a lower gain than that provided at 31 GHz). The mixer needs an LO drive power of around 12 dBm, so a gain of 30 dB must be provided by the booster board. All these calculations must be confirmed through measurements, which will be shown in Section 4.5.

IF and RF External Paths

This is a two way path, from TRX board to horn antenna, passing through the mixer. In the mixer, the LO signal is used to up-convert the IF signal and down-convert the RF signal. An schematic image of this path is given in Fig. 4.25. The mixer is the most important component of this path, because of its role in up/down-converting signals. The properties of the mixer are listed below:

- Conversion Loss: typically 8.5 dB, maximum 12.5 dB.
- LO-to-RF Isolation: 28 dB.
- LO-to-IF Isolation: 20 dB.

- RF-to-IF Isolation: 40 dB.
- Input 1dB Compression: 2 dBm.
- LO drive level: 9 to 14 dBm.

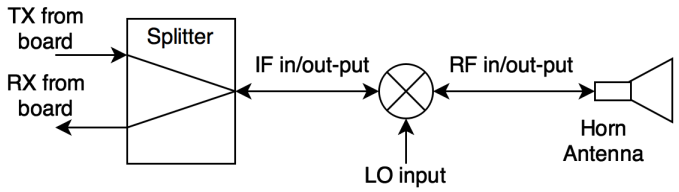

Figure 4.25: IF/RF path between TRX board and horn antenna.

Another component to take into account is the splitter, which (theoretically) has a 3dB transmission loss in every direction. In this kind of setups, it is better to use a circulator, which allows for transmission and reception, providing each port with sufficient protection. As an improvement, we propose to collocate a narrow band-pass filter, centered at 28 GHz, at the RF output of the mixer, in order to improve the quality of the transmitted and received signals.

Over-the-air (OTA) Propagation Path

This is a two-way propagation path, with the air as its physical medium. It is, ideally, a free-space propagation environment. The signal is sent over-the-air from the radio module to the horn antenna, and vice-versa. A conceptual image is shown in Fig. 4.26.

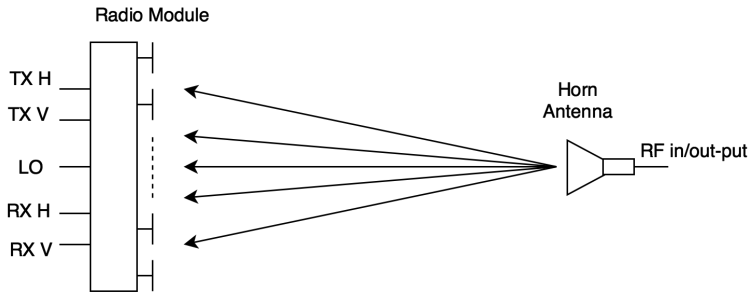

Figure 4.26: OTA propagation path between DUT and horn antenna.

The horn antenna has a gain of 15 dBi at 28 GHz. Each patch antenna in the radio module has a gain of 5 dBi. The free-space propagation loss, for far-field distances, follows Eq. 4.6; where d is the measurement distance, f is the working frequency and c is the speed of light in the air. The propagation loss at 28 GHz, with regard to d, can be seen in Fig. 4.27.

$$PL_{free-space}\ (dB) = 20 \cdot log_{10}\left(\frac{4\pi \cdot d \cdot f}{c}\right) \tag{4.6}$$

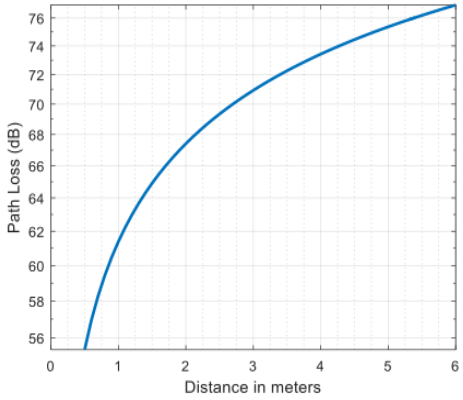

Figure 4.27: OTA free-space propagation loss at 28 GHz (valid from FF distance).

The OTA measurements from the horn antenna to the radio module must be performed at a distance further than the far-field (FF) distance, in order to ensure plane wave acquisition. The FF distance can be calculated by using Eq. 4.7, where D is the diameter of the smallest sphere that fully contains the antenna, and $\lambda = \frac{c}{f}$ is the wavelength in the air.

$$FF_{distance}\ (m) = \frac{2 \cdot D^2}{\lambda} \tag{4.7}$$

The diameter of the smallest sphere that fully contains the radio module is $D \approx 7cm$. Consequently, the far-field distance is 83 cm. The diameter of the sphere fully containing the horn antenna is 4.5 cm, so the measurement distance was set to 83 cm. The total effective loss in the OTA propagation path is $L_{tot} = PL_{free-space} - G_{patch} - G_{horn}$, where G_{patch} is the gain of each patch antenna and G_{horn} is the gain of the horn antenna. At 1 m distance, the total loss is $L_{tot} = 61 - 5 - 15 = 41$ dB. Depending on the direction of the measurement, the power at each antenna port can be calculated as:

- Transmission from DUT to Horn: $P_{horn} = P_{patch} - L_{tot}$
- Transmission from Horn to DUT: $P_{patch} = P_{horn} - L_{tot}$

It was decided that a received input power of -40 dBm was desirable in each measurement. A measurement distance of 4 m was chosen to ensure plane wave acquisition. The propagation loss was then increased to 67 dB.

4.4.3 Measurements Strategy

A description of the OTA measurements to be performed in the testbed is given in this section. There exist some code capable of doing some of the tasks in the measurements. Therefore, this code will be re-used when possible and only changed when necessary. A total of three sets of measurements are proposed.

Measurement 1

The first set of measurements is based on sending a plane wave from the probe antenna to the radio module's antenna. By measuring this plane wave in each patch element of the radio module, the RX circuits' responses can be estimated. A conceptual image of this set of measurements can be found in Fig. 4.28. In order to understand how these measurements are done in the testbed, all their steps are mentioned below. Synchronization requirements for the ADC and DAC can be found on Fig. 4.30. As well as this, a detailed flowchart describing this set of measurements is found in Fig. 4.31.

1. Default activation of the radio module and TRX board.
2. Launch test signal in the TRX board.
   (a) Activate the TRX board and the other external circuits.
   (b) Generate the local oscillator (LO) signal.
3. Measure the RX paths in the radio module/ASIC.
   (a) Activate one RX path .
   (b) Sample with DAC (synchronize it to ADC).
   (c) Extract the raw data signal from ADC.
   (d) Repeat from 3a with the next RX path (until RXs completion).
4. Send measurements to the PC.

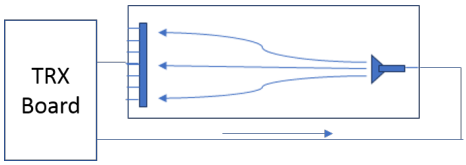

Figure 4.28: Conceptual image for the 1st measurement.

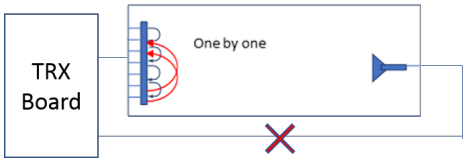

Figure 4.29: Conceptual image for the 2nd measurement.

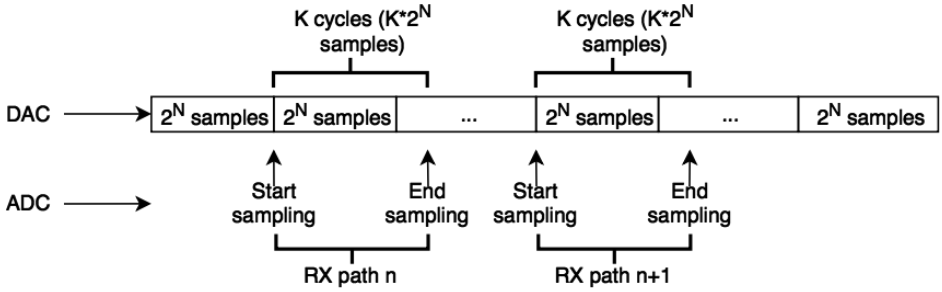

Figure 4.30: Synchronization requirement on ADC and DAC.

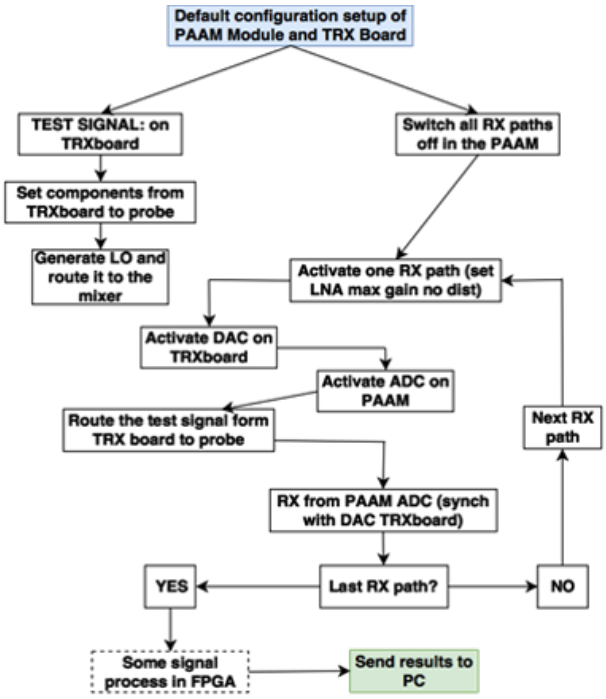

Figure 4.31: Flow chart for measurement 1.

Measurement 2

The second set of measurements consists of performing self-measurements between two antenna elements on the radio module. This set of measurements is done from one TX path to one RX path in the radio module. A conceptual image of this set of measurements can be found in Fig. 4.29. The steps to follow to perform this set of measurements are mentioned below. Synchronization requirements for the ADC and DAC can be found on Fig. 4.30. A very detailed flowchart containing the steps of measurement 2 is given in Fig. 4.32.

1. Default activation of the radio module.
2. Launch test signal in the radio module and generate the LO signal.
3. Measure the RX paths in the radio module/ASIC.
   (a) Activate one RX path and configure it.
   (b) Activate one TX path and configure it.
   (c) Sample with DAC (synchronize it to ADC).
   (d) Extract the raw data signal from ADC.
   (e) Repeat from 3b with the next TX path (until TXs completion).
   (f) Repeat from 3a with the next RX path (until RXs completion).
4. Send measurements to the PC.

Figure 4.32: Flow chart for measurement 2.

Measurement 3 (Validation)

The third set of measurements consists of pointing a maximum and a minimum of the radiation pattern to two different angular directions, both with and without calibration. This is done in both DL and UL transmission. Therefore, a total of 16 measurements will be performed. If the antenna array coupling matrix estimation and the calibration algorithms worked as planned, the system was expected to send more power in the maximums and less power in the minimums, with regard to a non-calibrated system. A conceptual image of this set of measurements can be found in Fig. 4.33.

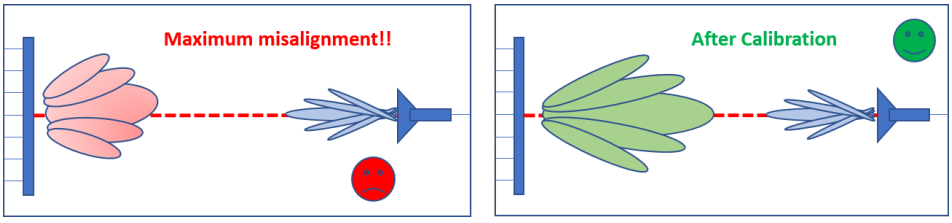

Figure 4.33: Conceptual image for third measurement.

4.4.4 Estimators and Measurements Correspondence

Array Coupling Matrix Estimation

Validation can be done by comparing the results obtained through measurements and estimators with the results obtained through simulations. The array coupling matrix estimation is performed by using the following sequence of processes:

1. Measurement 1 + RX path estimation, as it was done in Section 2.2.1.
2. Measurement 2 + relative DL to UL estimation.
3. Coupling matrix estimation.

Estimation and Compensation of TRX Circuits' Responses

For the calibration of the TRX circuits' responses, the following process is used:

1. Measurement 2 + absolute DL to UL estimation.
2. Compensation of the TRX circuits' responses.

The best way to validate this method is by using measurement 3, but another simpler procedure can be used. This simpler procedure consists of measuring the deviation of the TRX circuits' responses before and after calibration is performed. A lower deviation is expected when this measurement is conducted after the calibration has been applied.

4.5 HW External Path Measurements

In order to confirm the expected performance of the HW elements involved in the external paths in the testbed, some measurements using a vector network analyzer (VNA) and a spectrum analyzer (SA) must be conducted. By using these measurements, one can confirm the expected behaviour and also measure the real performance of the components. The aim is to measure each component separately, in order to verify their performance, and measure all of them connected together afterwards. Some unexpected issues caused delays:

- One of the supplied broadband amplifiers was broken.
- The provided comb-generator did not work well. A comparison of the performance of a correct one vs. that of the broken one is given in Fig. C.4.
- The cable to feed the booster board was not provided on time.
- The mechanical mounts of some components were not in place.

The broadband amplifiers and the BPF were measured using the VNA, and that is how the broken amplifier was detected. Several screen captures from the spectrum analyzer are shown in Appendix C.1, for an input signal of 0 dBm and 5.17 GHz. Even though the amplifiers were supposed to be fed with 7V and -0.3V for maximal gain performance, only 5V gave a similar performance and this

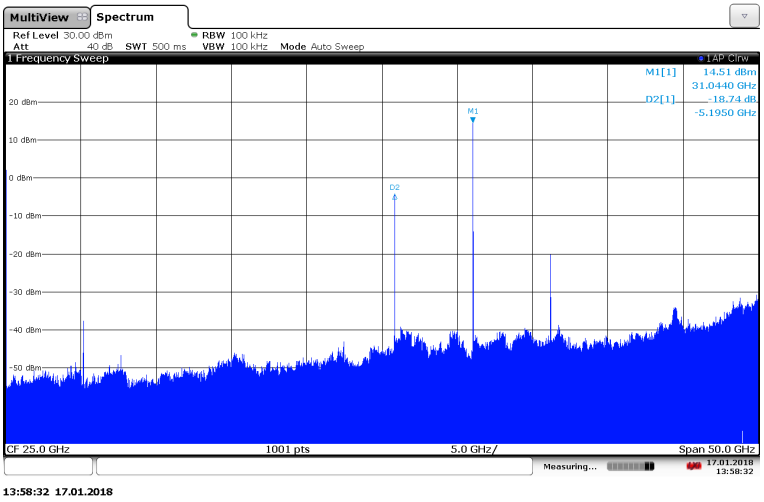

Figure 4.34: LO signal (output of booster board).

reduced the temperature of the components. Consequently, there was no need for extra cooling fans. In Fig. 4.34, one can find a measurement screen showing the output signal of the external LO path. There was a rejection of at least 18 dB between the wanted signal at 31 GHz and the spurious at 26 GHz and 36 GHz. Therefore, this signal can be taken as a pure enough LO signal.

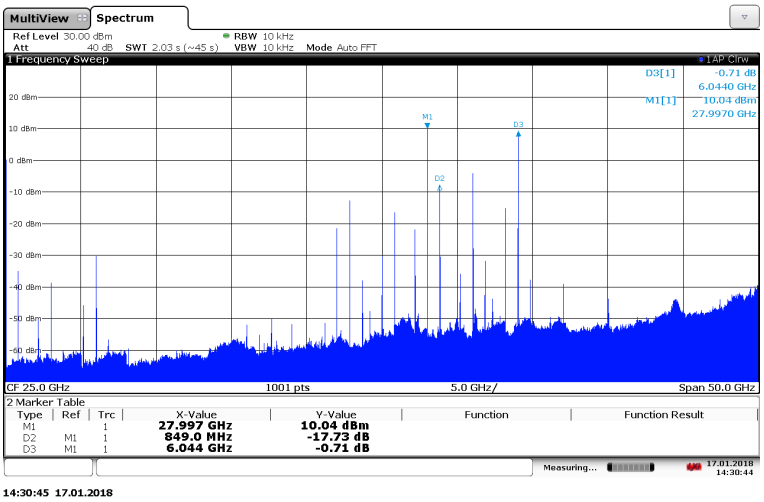

Figure 4.35: Booster board output, used after the mixer.

The generated LO tone at 31 GHz should have an amplitude between 9 and 14 dBm to properly drive the mixer. In Fig. 4.36, one can find a screen-shot of the SA, which shows the RF output of the mixer when a 10 dBm signal tone at 3 GHz was fed as an IF signal. In order to increase the RF output signal, the RF signal was

connected to the booster board to increase its power. The measurement results of this new setup is shown in Fig. 4.35. This setup with the booster board connected at the RF output would only be used for the set of OTA measurements. The power of the RF signal increased linearly as the power of the IF signal was increased, but only in the range from 0 dBm to 10 dBm. There was no substantial increase of the inter-modulation products in the mixer. Therefore, the power of the IF signal was set to 10 dBm. The TRX board provides with an IF signal of 0 dBm. Even though this power level was high enough for other calibration activities, they are not strong enough for the calibration and estimation activities in this work. Therefore, it is recommended that some power amplifiers should be used in the TX output of the TRX board.

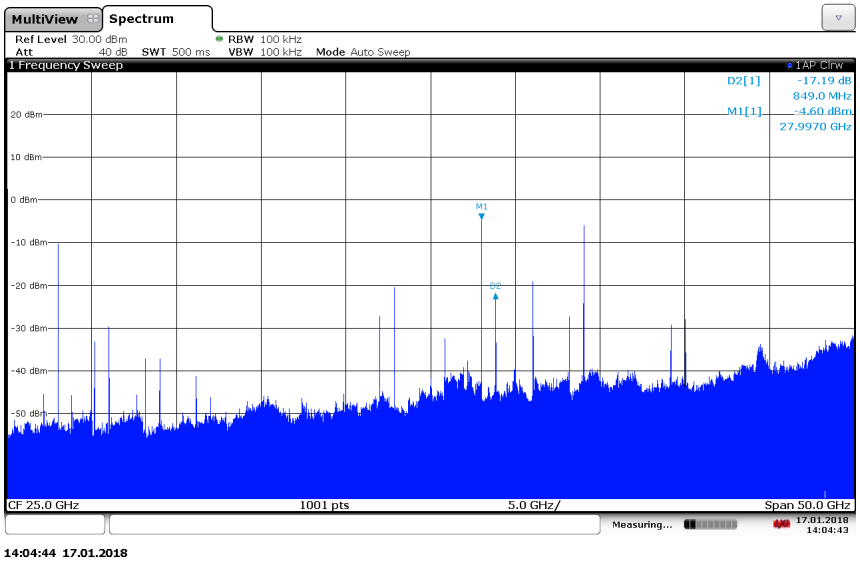

Figure 4.36: RF output of the mixer for the proposed setup.

The post-processing technique uses a cross-correlation calculation which increases the post-processing SNR by 60 dB. The noise level in the radio module receiver was around -77 dBm, so a 0 dBm input signal at the horn antenna will give an SNR of 30 dB, in each patch antenna port. With the post-processing gain, the SNR increases up to 90 dB. It was observed from simulations that the required SNR in order to properly estimate the antenna array coupling matrix was 90 dB. Thus, the HW is consistent with the requirements from simulations. Since the measurements will be performed at 4 m distance, the propagation loss is 67 dB. Taking into account the antennas gain, the total loss is 47 dB. A signal level of -40 dBm is desirable, so the input power at the horn antenna must be 7 dBm.

In order to estimate the antenna array coupling matrix, the maximum accuracy and quality of the signals must be determined. It is considered unusual that a BPF was not added at the output of the mixer. Therefore, a narrow-band BPF centered at ≈28 GHz was proposed to be added (Marki Microwave FB-2770) and it was connected to the RF port of the mixer.

4.6 Code Preparation and OTA measurements

To perform the validation measurements for the TRX circuits' calibration algorithms, it is necessary to write control codes for the radio module and the instruments in the testbed. A source code of several files containing some of the functions needed to control the instruments was provided. These functions were developed in previous calibration activities conducted in other premises of the company. These sources of code were written in three different programming languages (MATLAB, C# and Python), and this increased the difficulty of customizing these codes for measurements. Three main parts of code are needed. The first part is related to the control of the TRX board, which contains the digital base-band domain. This part is in charge of injecting a signal through several DAC ports and reading another signal from several ADC ports. A baseline code to perform this "inject + read" of the signals must be developed. The second part is related to the control of the radio module, which contains the RF circuitry. This part is in charge of activating and deactivating different TX and RX paths in the radio module. And the third part is related to the calibration algorithms and estimators, which is conducted in the PC. This part is in charge of performing the estimations and calibration using raw data from measurements. Therefore, regarding control and processing code, the following tasks must be completed:

- Write the baseline code to inject/read signals in the TRX board.
- Create the code for controlling the radio module, for each of the measurements defined in this work.
- Translate to Python the algorithms and estimators developed in this work. Write the code that combines the control of the radio module and the estimation algorithms.
- Develop the code for the validation measurements.

Some functions have been identified in the code provided. The functions which are related to the control of the radio module are: identification of the corresponding front-end (FE) and integrated circuit (IC) from a given element number, enabling the selected ICs and FEs, setting the LO, setting the polarization, setting the amplifiers (PA or LNA), setting the phase shifters and setting the beam pointing direction from a pre-stored set of directions. The functions related to control of the TRX board include: measurement of the delay and the complex scaling between one DAC and one ADC ports in the board, initialization of the FPGA and other functions which are not needed for the purpose of this work.

There was time to develop the baseline code for injection and reading of signals in the TRX board, between the selected DAC and ADC ports. An identification of its different ports was obtained and provided as well. here are 4 ADC ports as well as 6 DAC ports (2 of them used for the LO signal). Pseudo-code sources related to the third and fourth tasks outlined above are shown in Section C.3. Besides, a few self-measurements and plane wave acquisition measurements were conducted, to check it was possible to do so with the functionalities that were provided. From this point, it is almost straightforward to continue the measurements work.

Chapter 5

Conclusions and Future Work

5.1 Conclusions

Algorithms for TRX circuits' calibration have been studied and tested. These algorithms have been proven, through simulations, to improve the beamforming capabilities of antenna arrays. In order to validate their performance, a testbed has been set up. The initial aim was to measure an Ericsson's radio module on it, but because of a lack of time, this is left for future work. TRX calibration algorithms, in order to work, must use the antenna array coupling matrix coefficients. Hence, an innovative and efficient algorithm for the estimation of the antenna array coupling matrix has been studied and simulated. It has been proven that the calibration and estimation algorithms perform better with low levels of interference and high post-processing SNR values. So as to prepare the validation setup, the elements which were needed, were gathered and measured. To perform the validation measurements, several pieces of control code must be developed. The aim of these pieces of code is to configure and control all the equipment in the testbed setup. This part of the thesis could not be completed due to limited time and factors outside the control of the project. Despite this, a baseline code capable of performing some of the required tasks has been prepared and explained in this thesis work.

Beamforming in an antenna array is achieved by changing the complex signals that excite each antenna element in the array. When pointing the beam, the effect of the phase component is much more important than the effect of the amplitude component. Algorithms for TRX calibration have shown to better correct the phase component than the amplitude component (as can be observed in Fig. B.1), and that is why these algorithms are very convenient for the improvement of beamforming capabilities. In these algorithms, the TRX circuits' responses must be estimated. Self-measurements, which consist of transmitting through each antenna element and receiving in each of the other antenna elements, must be conducted over the antenna array. These measurements are then used in an algorithm which estimates the TRX circuits' responses. Both linear and non-linear estimation techniques have been studied and simulated. The main conclusion is: the least amount of the strongest self-measurements must be used in the estimation phase. This approach offers two advantages: less measurements are used (lower time to make them) and less computation resources for the estimation.

Regarding the antenna array mutual coupling matrix estimation, two measurements are needed: plane wave acquisition in the radio module and self-measurements over the same radio module. The noise in the first measurement acts as interference in the estimation, while the noise in the second measurement acts as AWGN. Both measurements were affected by a deterministic component of interference, but this was simulated as a reciprocal interference. That is the reason why it did not affect the performance of the estimation. If the interference is regarded as reciprocal and invariant in time, the estimation will lead to both the antenna array coupling matrix and the interference. Some more simulations considering a non-reciprocal interference should be made. The provided radio module has some connection-related limitations that must be taken into account when conducting self-measurements. TRX circuits' calibration algorithms must be customized to specific systems. The HW elements provided to compose the testbed had been measured. It is concluded that the initially proposed setup can be improved by adding some extra amplifiers and an extra filter. Regarding the control code, some modifications, over an already existing code, have been done. The main contributions are a baseline code and an explanation on how to develop the necessary programs to conduct the OTA measurements.

5.2 Future Work

5.2.1 Calibration Algorithms

Some ideas related to the algorithms for TRX circuits' calibration include:

- Use orthogonal codes from each transmit antenna to all the receive antennas, to allow for parallel self-measurements.
- Solve LLS estimation by using Lagrange Multipliers. This is explained in section 2.1.
- Create a mixed estimation of weighted and neighbour methods.
- Apply Control Theory to the calibration procedure, which is combined with the simulation of a dynamic system. This is explained below.
- Develop calibration algorithms for distributed massive MIMO networks. This idea is also explained below.

Dynamical System and Control Theory

It is interesting to simulate a dynamical system in order to check how a measurement delay may affect the compensation performance. This happens since small changes in the TRX circuits' responses can happen in the time the system takes to perform all the self-measurements, leading to an estimation that is not a 100% correct. If the self-measurements are performed over a very long time span, the TRX circuits' responses may have changed significantly, as is depicted on the left image of Fig. 5.1. If Control Theory is applied, a variant of the calibration procedure can be defined. By doing so, the system can track the changes in the

responses, as it is shown on the right image of Fig. 5.1. The crosses show how the TRX chain responses of the system changes. The dots show how well the chain responses are estimated. The circle shows the possible values to which the estimation can "jump", depending on the measurement time. The longer the measurement time, the smaller and closer to the results the circle is. A combination of actual and previous measurements can be used in the estimation. As well as this, one can use a combination of previous and actual estimations. Fig. 5.2 and Fig. 5.3 show possible control loops to use in the calibration procedure, but this idea must be much further developed.

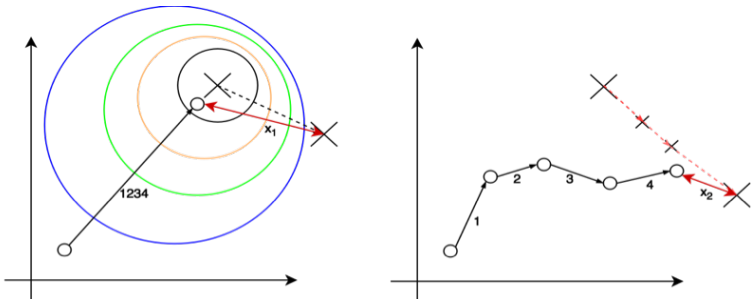

Figure 5.1: Long (left) vs short (right) time measurements applying control theory.

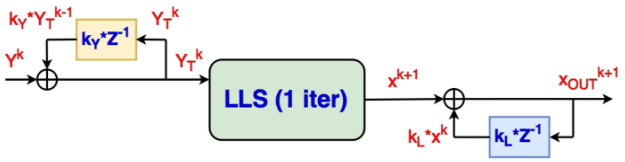

Figure 5.2: Control theory loop for LLS calibration.

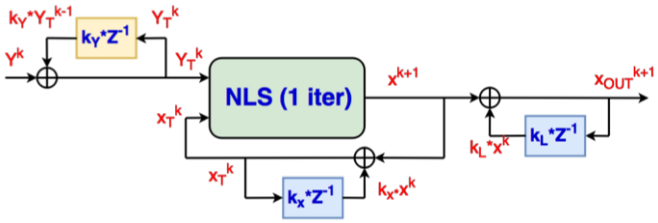

Figure 5.3: Control theory loop for NLLS calibration.

Application of Calibration Algorithms to Distributed Massive MIMO Networks

The calibration algorithms shown in this work can only be applied to single arrays. Distributed massive MIMO networks, which are composed of various co-

operating arrays, will be used in 5G systems. Because of the unknown constant that appears in the estimation algorithms, if each array is calibrated independently, advanced wireless techniques such as coordinated multi-point can not be used. Each antenna array would receive/send signals with different phase values in reception/transmission. Therefore, the TRX circuits' responses of all the arrays must be estimated together in a common processing unit, since this will overcome the difference in unknown constants, creating a common constant for all the arrays. This concept is similar to the one of neighbour measurements, and this is shown in Fig. 5.4. A base-station can be seen as the sub-array of an array in the cooperating system. Simulations to confirm the viability of this idea must be conducted.

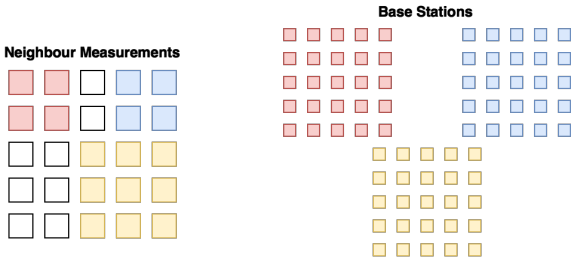

Figure 5.4: Parity between sub-arrays and base-stations using neighbour measurements for TRX chain responses estimation.

5.2.2 Array Coupling Matrix Estimation

Only one of the two proposed estimation methods shown to work correctly. Since the second one (that failed to work) seemed more appropriate, an attempt can be made to solved the problem, such as using Lagrange multipliers on it. Apart from this, simulations considering non-reciprocal interference must be done, in order to analyze its impact on the estimation performance. Besides, it is suggested that the elements with the strongest coupling gains in the self-measurements involved in this estimator, since this can help to increase the performance.

5.2.3 Over-The-Air (OTA) Measurements

It is recommended to acquire a BPF centered at 28 GHz, and put it at the RF output of the mixer. Some preparation of the code to perform the OTA measurements has been done, but there was not enough time to prepare everything. A baseline code has been developed, apart from a detailed description on how to write and perform the OTA measurements. It is recommended to develop all the code in Python, to avoid an increase in the complexity, coming from the communications between different programming languages. Hence, future work includes: translate the algorithms developed in MATLAB, write code to control the radio module, perform the measurements in an an-echoic chamber and compare results with the simulations in this work.

Bibliography

[1] *"Ericsson 5G perspective"*, https://www.ericsson.com/en/5g

[2] *"Qualcomm 5G"*, https://www.qualcomm.com/invention/5g

[3] *"Mitsubishi Electric's New Multibeam Multiplexing 5G Technology Achieves 20Gbps Throughput"*, 21 January 2016, http://www.mitsubishielectric.com/news/2016/0121.html

[4] E. G. Larsson, O. Edfors, T. L. Marzetta, *"Massive MIMO for Next Generation Wireless Systems"*, IEEE Communications Magazine, Feb. 2014.

[5] J. Winters, *"On the Capacity of Radio Communication Systems with Diversity in a Rayleigh Fading Environment"*, IEEE Journal on Selected Areas in Communications, vol. SAC-5, pp. 871 -878, Jun. 1987.

[6] L. Lu, G. Y. Li, A. Lee, A. Ashikhmin, R. Zhang, *"An Overview of Massive MIMO: Benefits and Challenges"*, IEEE Journal of Selected Topics in Signal Processing, vol. 8, no. 5, Oct. 2014.

[7] T. S. Rappaport, S. Sun, R. Mayzus, H. Zhao, Y. Azar, K. Wang, G. N. Wong, J. K. Schulz, M. Samimi, F. Gutierrez, *"Millimeter Wave Mobile Communications for 5G Cellular: It Will Work!"*, IEEE Access, vol. 1, 2013.

[8] T. E. Bogale, L. B. Le, *"Massive MIMO and mmWave for 5G Wireless HetNet"*, IEEE Vehicular Technology Magazine, Mar. 2016.

[9] U. Gustavsson, C. Sanchez Perez, T. Eriksson, F. Athley, G. Durisi, P. Landin, K. Hausmair, C. Fager, L. Svensson, *"On the Impact of Hardware Impairments on Massive MIMO"*, Globecom 2014, IEEE, 8-12 Dec. 2014.

[10] J. Vieira, F. Rusek, F. Tufvesson, *"Reciprocity Calibration Methods for Massive MIMO based on Antenna Coupling"*, Globecom 2014, IEEE, 8-12 Dec. 2014.

[11] J. Vieira, F. Rusek, O. Edfords, S. Malkowsky, L. Liu, F. Tufvesson, *"A Receive/Transmit Calibration Technique based on Mutual Coupling for Massive MIMO Base Stations"*, IEEE 27th Annual International Symposium on PIMRC, 4-8 Sept. 2016.

[12] J. Vieira, F. Rusek, F. Tufvesson, *"Reciprocity Calibration for Massive MIMO: Proposal, Modeling, and Validation"*, IEEE Transactions on Wireless Communications, vol. 16, no. 5, May 2017.

[13] H. Wey, D. Wang, H. Zhu, J. Wang, S. Sun, X. You, *"Mutual Coupling Calibration for Multiuser Massive MIMO Systems"*, IEEE Transactions on Wireless Communications, vol. 15, no. 1, Jan. 2016.

[14] M. Mowler, E. G. Larsson, B. Lindmark, B. Ottersten, *"Methods and Bounds for Antenna Array Coupling Matrix Estimator"*, IEEE International Conference on Acoustics, Speech and Signal Processing, 2007.

[15] B. Sadhu, Y. Tousi, J. Hallin, S. Sahl, S. K. Reynolds, Ö. Renström, K. Sjögren, O. Haapalahti, N. Mazor, B. Bokinge, G. Weibull, H. Bengtsson, A. Carlinger, E. Westesson, J. E. Thillberg, L. Rexberg, M. Yeck, X. Gu, M. Ferriss, D. Liu, D. Friedman, and A. Valdes-Garcia, *"A 28-GHz 32-Element TRX Phased-Array IC With Concurrent Dual-Polarized Operation and Orthogonal Phase and Gain Control for 5G Communications"*, IEEE Journal of Solid-State Circuits, vol. 52, no. 12, Dec 2017.

[16] Joakim Hallin, *"Testbed Development"*, Ericsson Internal.

[17] H. Jidhage, O. Nystrom, *"Antenna Calibration"*, Ericsson Internal.

[18] T. Carlsson, *"Antenna Calibration and Validation"*, Ericsson Internal.

[19] T. Carlsson, *"Antenna Factory Calibration"*, Ericsson Internal.

[20] J. M. Martinez, *"Practical Quasi-Newton Methods for solving Nonlinear Systems"*, Journal of Computational and Applied Mathematics, vol. 124, pp. 97-121, Jan. 2000.

[21] C. A. Balanis, *"Antenna Theory: Analysis and Design"*, Wiley, 2005

[22] F. Kaltenberger, H. Jiang, M. Guillaud, and R. Knopp, *"Relative Channel Reciprocity Calibration in MIMO/TDD systems"*, Future Network and Mobile Summit, Jun. 2010.

[23] A. Hall, *"Generalized Method of Moments"*, Advanced Texts in Econometrics. Oxford, 2004.

[24] *"Lagrange Multipliers"*, Wikipedia, https://en.wikipedia.org/wiki/Lagrange_multiplier

[25] J. L. Masa-Campos, J. M. Fernandez, M. Sierra-Castañer, M. Sierra-Perez, *"Coupling Characterization and Compensation Model for Antenna Arrays"*, Journal of Microwaves and Optoelectronics, Vol. 4, No. 2, Dec 2005.

Appendix A

Full Derivation of Estimators

A.1 Full Derivation of LLS Estimator

The signal model for the TRX circuits' calibration is as follows $\mathbf{y}_{n,m} = \mathbf{r}_n \cdot (\overline{\mathbf{h}}_{n,m} + \widetilde{\mathbf{h}}_{n,m}) \cdot \mathbf{t}_m + \mathbf{n}_{n,m}$. By considering $SNR \to \infty$ and $SIR \to \infty$, the previous equation is simplified to $\mathbf{y}_{n,m} = \mathbf{r}_n \cdot \overline{\mathbf{h}}_{n,m} \cdot \mathbf{t}_m$, which can be defined as:

$$\Gamma_{n,m} = \frac{\overline{\mathbf{h}}_{n,m}}{\mathbf{y}_{n,m}} = \frac{1}{\mathbf{r}_n} \cdot \frac{1}{\mathbf{t}_m} \to \Gamma_{n,m} \cdot \mathbf{t}_m - \frac{1}{\mathbf{r}_n} = 0. \tag{A.1}$$

Equation A.1 can be re-written in the matrix form $\mathbf{A} \cdot \mathbf{x} = \mathbf{b}$. The formulation of matrix $\mathbf{A}$ is found below in Eq. A.2.

$$\mathbf{A} = \begin{pmatrix} 0 & \Gamma_{21} & 0 & \dots & 0 & -1 & 0 & \dots & 0 \\ 0 & 0 & \Gamma_{31} & \dots & 0 & -1 & 0 & \dots & 0 \\ \vdots & \vdots & \vdots & \ddots & 0 & \vdots & \vdots & \ddots & \vdots \\ \Gamma_{12} & 0 & 0 & \dots & 0 & 0 & -1 & \dots & 0 \\ 0 & \Gamma_{32} & 0 & \dots & 0 & 0 & -1 & \dots & 0 \\ \vdots & \vdots & \vdots & \ddots & \vdots & \vdots & \vdots & \ddots & \vdots \\ 0 & 0 & 0 & \dots & \Gamma_{M(M-1)} & 0 & 0 & \dots & -1 \\ 1 & 0 & 0 & \dots & 0 & 0 & 0 & \dots & 0 \end{pmatrix} \tag{A.2}$$

The vector $\mathbf{x}$ contains the unknowns $\mathbf{t}_m$ and $\frac{1}{\mathbf{r}_n}$, as it is seen in $\mathbf{x} = [1/r_1 = 1,\ 1/r_2 = 1,\ \dots\ 1/r_M = 1,\ t_1\ t_2\ \dots\ t_M]^T$, and b has only one element different from zero, to avoid the all-zero solution, as seen in $b = [0,\ 0,\ 0,\ \dots,\ 1]^T$. Vector $\mathbf{x}$ would be calculated as $\mathbf{x} = (\mathbf{A}^T\mathbf{A})^{-1}\mathbf{A}^T \cdot \mathbf{b}$. With the previous formulation, if only neighbour measurements are used, one must remove the rows corresponding to measurements which have not been performed, both in matrix A and vector b.

Regarding the definition of the previous equations, there are two possibilities. Define $\Gamma_{n,m} = \frac{\overline{\mathbf{h}}_{n,m}}{\mathbf{y}_{n,m}}$ or $\Gamma_{n,m} = \frac{\mathbf{y}_{n,m}}{\overline{\mathbf{h}}_{n,m}}$. In the first case, the equivalent post-processing noise formulation can be found in Eqs. A.3 and A.4. In the second case, the

equivalent noise can be found in Eq. A.5.

$$\Gamma_{n,m} = \frac{\overline{\mathbf{H}}}{\mathbf{y}_{noise}} = \frac{\overline{\mathbf{H}}}{\mathbf{y}_{no-noise}} + N' \rightarrow N' = -\frac{N \cdot \mathbf{H}}{\mathbf{y}_{no-noise}(\mathbf{y}_{no-noise} + N)} \tag{A.3}$$

$$N' = -\frac{N \cdot \mathbf{H}}{\mathbf{y}_{no-noise}(\mathbf{y}_{no-noise} + N)} = -\frac{N}{\mathbf{R} \cdot \mathbf{T} \cdot (\mathbf{R} \cdot \mathbf{H} \cdot \mathbf{T} + N)} \tag{A.4}$$

$$\Gamma_{n,m} = \frac{\mathbf{y}_{noise}}{\overline{\mathbf{H}}} = \mathbf{R} \cdot \mathbf{T} + N'' \rightarrow N'' = \frac{N}{\mathbf{H}} \tag{A.5}$$

It can be seen that $N' \ll N''$ in case $\mathbf{R} \gg \mathbf{1}$ and $\mathbf{T} \gg \mathbf{1}$. Since TX and RX chains are set to their maximum gains, the first option is the best.

A.2 Full Derivation of NLLS Estimator

We must define a set of equations in vector form as $\mathbf{f}(\mathbf{x}) = \mathbf{b} = \mathbf{0}$, i.e.

$$\begin{bmatrix} f_1(\mathbf{x}) \\ f_2(\mathbf{x}) \\ \vdots \\ f_K(\mathbf{x}) \end{bmatrix} = \begin{bmatrix} 0 \\ 0 \\ \vdots \\ 0 \end{bmatrix}, \tag{A.6}$$

where $\mathbf{x}$ is the vector of unknowns. The vector $\mathbf{x}$ can be found by iterations $\mathbf{x}_{l+1} = \mathbf{x}_l - \mathbf{J}(\mathbf{x}_l)^+ \cdot \mathbf{f}(\mathbf{x}_l)$, where J^+ is the pseudo-inverse of the Jacobian matrix. The function $f(x)$is defined as $f_{n,m} = \Delta_{n,m} - \delta t_m \cdot \delta r_n$, with

$$\Delta_{n,m} = \frac{\overline{h}_{n,m}}{y_{n,m}}, \quad \delta t_m = \frac{1}{t_m} \quad and \quad \delta r_n = \frac{1}{r_n}. \tag{A.7}$$

The Jacobian matrix is $[\mathbf{J}(x_l)]_{mn} = \frac{\partial f_m}{\partial x_n}$, where $m = 1 \dots M$ is the number of equations and $n = 1 \dots N$ is the number of unknowns. Vector $\mathbf{x}$ equals $\mathbf{x} = [\delta r_1,\ \delta r_2,\ \dots \delta r_M,\ \delta t_1,\ \delta t_2,\ \dots \delta t_M]^T$. The full formulation of the Jacobian matrix is found in Eq. A.8,

$$\mathbf{J} = \begin{bmatrix} 0 & \delta t_1 & 0 & \dots & 0 & 0 & -\delta r_2 & 0 & \dots & 0 \\ 0 & 0 & \delta t_1 & \dots & 0 & 0 & -\delta r_3 & 0 & \dots & 0 \\ \vdots & \vdots & \vdots & \ddots & \vdots & \vdots & \ddots & \vdots & \vdots & \\ 0 & 0 & 0 & \dots & 0 & \delta t_1 & -\delta r_M & 0 & \dots & 0 \\ \delta t_2 & 0 & 0 & \dots & 0 & 0 & 0 & -\delta r_1 & \dots & 0 \\ 0 & 0 & \delta t_2 & \dots & 0 & 0 & 0 & -\delta r_3 & \dots & 0 \\ \vdots & \vdots & \vdots & \ddots & \vdots & \vdots & \vdots & \ddots & \vdots & \vdots \\ 0 & 0 & 0 & \dots & 0 & \delta t_2 & 0 & -\delta r_M & \dots & 0 \\ -\delta t_M & 0 & 0 & \dots & 0 & 0 & 0 & 0 & \dots & -\delta r_1 \\ \vdots & \vdots & \vdots & \ddots & \vdots & \vdots & \vdots & \ddots & \vdots & \vdots \\ 0 & 0 & 0 & \dots & -\delta t_M & 0 & 0 & 0 & \dots & -\delta r_{M-1} \end{bmatrix}. \tag{A.8}$$

Appendix B

Additional Simulations

B.1 Additional Simulation Results for the Calibration Method

In this section, there are several figures which show the amplitude and phase of the complex TX and RX responses, both before and after calibration. One and two iterations are represented. Both LLS and NLLS estimation are represented as well.

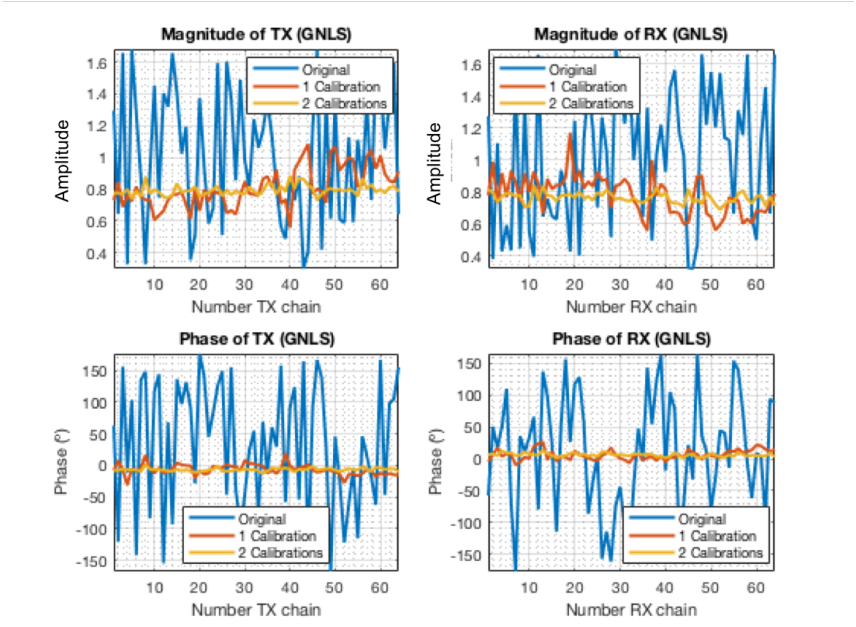

Figure B.1: NLLS, SNR = 40 dB, no interference, TX and RX vector responses. Blue for uncalibrated, red and yellow for calibrated.

B.2 Additional Simulation Results for the Coupling Matrix Estimator

In this section, some images of the results of the antenna array mutual coupling estimation, by using the first method proposed by Ericsson, can be found. It is important to control the values of SNR_{RX} and SNR_{SM} in order to avoid undesired (but not erroneous) results.

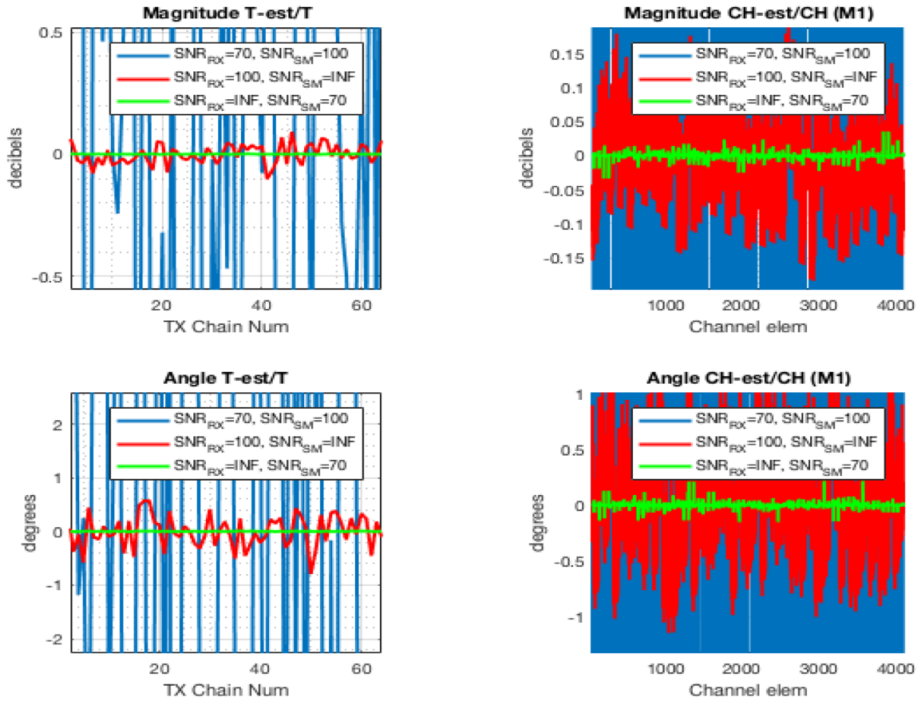

Figure B.2: Antenna coupling estimation given different SNRs in Plane Wave Acquisition and Self-measurements (T and CH).

Appendix C

Additional Information: Testbed and Radio Module

C.1 Additional Information on the Testbed

By observing Fig. C.6, one can see little but noticeable differences in the responses of both comb generators. The one which is considered as broken works, but worse than expected.

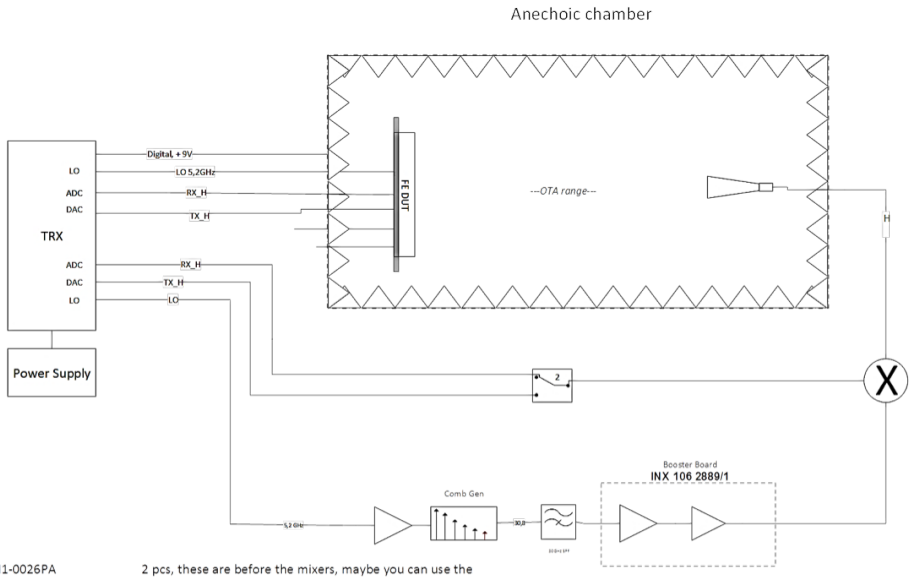

ADM1-0026PA	2 pcs, these are before the mixers, maybe you can use the two remaining TX paths from the booster board to get more pout.
FB-3270	BPF at 31 GHz
DBPD0204000800A	power divider at 5 GHz, you probably have this one in stock
DBPD0226504000A	power divider at 28 GHz, you may have in stock
M9-0540LN	2 pcs, mixers
NLTL-6026S	Comb generator

Figure C.1: Schematic of the testbed setup.

Component	N	ID	Manufacturer	Source	Comments
Radio ASIC	one	one	Ericsson	Internal	
TRX Board	one	two	Ericsson	Internal	
BB Amplifier	one	three	Marki Mic.		<26.5GHz. Sat. out 20dBm. G = 12dB.
Mixer	one	4	Marki Microw.		Input CP 2dBm, Loss -7.5dB. LO to RF isol. -30dB, LO level 13-18dBm.
Comb gener.	one	5	Marki Mic.		Min input 16dBm. 6th harm. -30 dB.
31 GHz BPF	one	6	Marki Mic.		Passband loss 2.5 dB, 9 GHz BW
28 GHz Amp	one	7	Ericsson	MIC	Booster board, several amplifiers.
Test fixture	one	8	Ericsson	MIC	
Horn Antenna	one	9	?	Internal	
Cables	three	10	?	Internal	Loss not critical, one two m, too short
RF Switch	one	11	?	Internal	GPIB controlled
Power supply	one	12		Internal	Manually controlled
Test PC	one	13		Internal	Verify LAN board and MATLAB.

Table C.1: Components for testbed system. Some already available, others acquired.

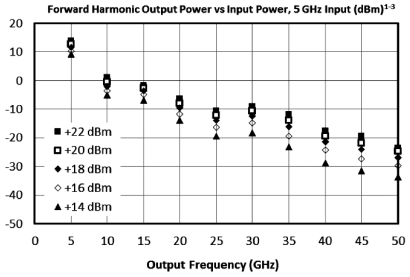

Figure C.2: Comb generator response for a 5 GHz input signal.

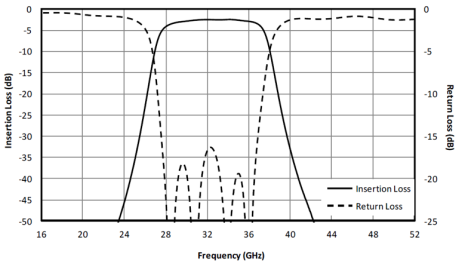

Figure C.3: Frequency response of the BPF at 32 GHz.

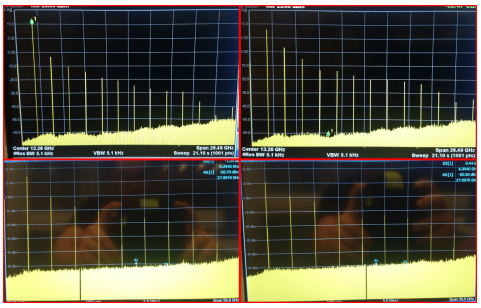

Figure C.4: Broken comb-generator (left) and unbroken (right). Top is two GHz input and bottom is 5 GHz.

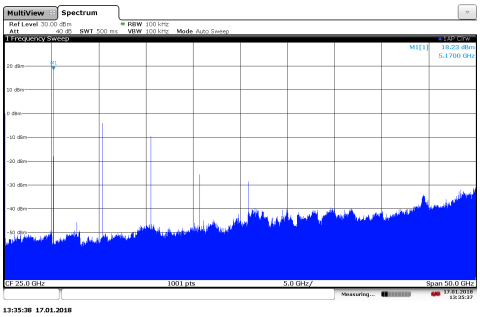

Figure C.5: Output of 2 broadband amplifiers connected in series.

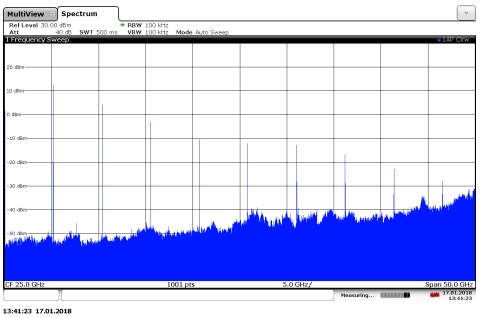

Figure C.6: Output of comb generator connected to the two broadband amplifiers. 5 GHz divisions.

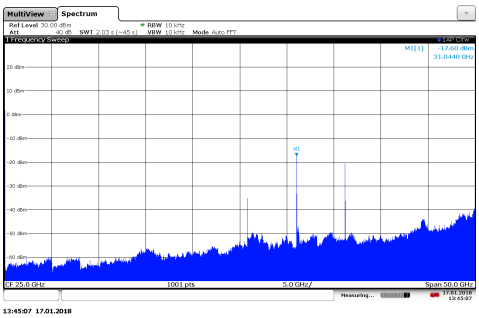

Figure C.7: Output of band pass filter connected to previous chain. 5 GHz divisions.

C.2 Additional Information of the Radio Module

A picture of the radio module to be used for validation measurements can be found in Fig. C.8. On the back of the radio module, there are 5 RF connections and one pins connection. The 5 RF connections correspond to TX horizontal, TX vertical, RX horizontal, RX vertical and the LO (local oscillator). The pins connection is used for control purposes, i.e. communication between the TRX board and the radio module. This control is in charge of activating the radio module, controlling the power amplifiers and low-noise amplifiers, activating and deactivating different TRX chains, etc.

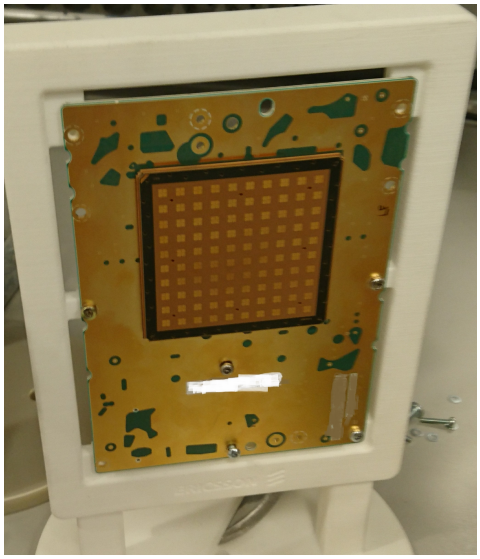

Figure C.8: Picture of the radio module from broadside direction.

C.3 Pseudo-code for OTA Measurements

This section contains a pseudo-code description of the control codes for performing measurement 1 and measurement 2 of the OTA measurements defined in this work.

The first measurement is related to the estimation of the RX circuits' responses, for its use in the estimation of the antenna array coupling matrix. The second measurement is related to the estimation of the TRX circuits' responses (either absolute or relative responses) using self-measurements performed in the radio module.

Algorithm 1 Measurement 1

procedure READ RX PATHS COMPLEX RESPONSES
Initialization
    DAC = dac ← Set DAC to one connected to PAAM
    ADC = adc ← Set ADC to the one connected to horn antenna
    REF = measReference(DAC,ADC) ← Measure reference element
loop 1 (over RX paths):
    activateRXpath(iter) ← Activate DUT's corresponding RX path
    measRx(iter) = measAmpPh(DAC,ADC,REF) ← Read scaling
close loop;
    estRXpaths = estimRX(measRx) ← Estimate RX paths using
end.

Algorithm 2 Measurement 2

procedure SELF-MEASUREMENTS IN RADIO MODULE
Initialization
    DAC = dac ← Set DAC to one connected to PAAM
    ADC = adc ← Set ADC to one connected to PAAM
    REF = measReference(DAC,ADC) ← Measure reference element
loop 1 (over RX paths):
    activateRXpath(iter1) ← Activate DUT's RX corresponding path
loop 2 (over TX paths):
    activateTXpath(iter2) ← Activate DUT's TX corresponding path
    measRxTx(iter1,iter2) = measAmpPh(DAC,ADC,REF) ← Scaling
close loop 2;
close loop 1;
    estRX2TXpaths = estimRX2TX(measRxTx) ← RX to TX response
    estRXTXpaths = estimRXTX(H,measRxTx) ← RX and TX responses
end.